Article:
Su, X, Wu, T, Zhang, J et al. (9 more authors) (2022) Present-Day PM2.5 over Asia: Simulation and Uncertainty in CMIP6 ESMs. Journal of Meteorological Research, 36 (3). pp. 429-449. ISSN 2095-6037

https://doi.org/10.1007/s13351-022-1202-7

Present-Day $PM_{2.5}$ in Asia: Simulation and Uncertainty in CMIP6 ESMs

Xiaole SU[1,2], Tongwen WU[1,2*], Jie ZHANG[2], Yong ZHANG[1,3], Junli JIN[3], Qing ZHOU[3], Fang ZHANG[2], Yiming LIU[2], Yumeng ZHOU[1,2], Lin ZHANG[4], Steven T. TURNOCK[5,6], and Kalli FURTADO [5]

1 *Chinese Academy of Meteorological Sciences, China Meteorological Administration, Beijing* 100081, *China*

2 *Beijing Climate Center, China Meteorological Administration, Beijing* 100081, *China*

3 *Meteorological Observation Center, China Meteorological Administration, Beijing* 100081, *China*

4 *Laboratory for Climate and Ocean-Atmosphere Studies, Department of Atmospheric and Oceanic Sciences, School of Physics, Peking University, Beijing* 100871, *China*

5 *Met Office, Hadley Centre, Exeter* EX1 3PB, *United Kingdom*

6 *University of Leeds Met Office Strategic (LUMOS) Research Group, School of Earth and Environment, University of Leeds, Leeds* LS2 9JT, *United Kingdom*

Submitted November 21, 2021

Supported by the National Key Research and Development Program of China (2016YFA0602100), and the UK-China Research & Innovation Partnership Fund through the Met Office Climate Science for Service Partnership (CSSP) China as part of the Newton Fund.

* Corresponding author: twwu@cma.gov.cn. Tel: 13651180792

ABSTRACT

This study assesses the ability of ten Earth System Models (ESMs) that participated in Phase 6 of the Coupled Model Intercomparison Project (CMIP6) to reproduce the present-day inhalable particles with diameters less than 2.5 micrometers ($PM_{2.5}$) over Asia and discusses the uncertainty. $PM_{2.5}$ accounts for more than 30% of the surface total aerosol (fine and coarse) concentration over Asia, except for Central Asia. The simulated spatial distributions of $PM_{2.5}$ and its components, averaged for the period from 2005 to 2020, are consistent with the Modern-Era Retrospective Analysis for Research and Applications version 2 (MERRA-2) reanalysis. They are characterized by the high $PM_{2.5}$ concentrations over eastern China and northern India where anthropogenic components such as sulfate and organic aerosol dominate, and in northwestern China where the mineral dust in $PM_{2.5}$ fine particles ($PM_{2.5}DU$) dominate. The present-day multi-model mean (MME) $PM_{2.5}$ concentrations slightly underestimate ground-based observations in the same period of 2014-2019, although observations are affected by the limited coverage of observation sites and the impact of urban areas. Those model biases partly come from other aerosols (such as nitrate and ammonium) not involved in our analyses, and also are contributed by large uncertainty in $PM_{2.5}$ simulations on local scale among ESMs. The model uncertainties over East Asia are mainly attributed to sulfate and $PM_{2.5}DU$; over South Asia they are attributed to sulfate, organic aerosol and $PM_{2.5}DU$; over Southeast Asia they are attributed to sea salt in $PM_{2.5}$ fine particles ($PM_{2.5}SS$); and over Central Asia they are attributed to $PM_{2.5}DU$. They are mainly caused by the different representations of aerosols within individual ESMs including the representation of aerosol size distributions, dynamic transport, physical and chemistry mechanisms.

Keywords: $PM_{2.5}$, Asia, CMIP6, Earth System Models

Citation: Su, X. L., T. W. Wu, J. Zhang, et al., 2017: Present-day PM2.5 in Asia: simulation and uncertainty in CMIP6 ESMs. *J. Meteor. Res.,* **36**(x), XXX－XXX, doi: 10.1007/s13351-022-0xxx-x.

1. Introduction

Aerosol is a multiphase system composed of solid particles and liquid droplets, suspended in a gaseous carrier phase (e.g., air). Atmospheric aerosols can include minerals (e.g., silicates) originating from soils and rocks, carbonaceous components (black carbon and organic carbon), sulfates, nitrates, ammonium salts, sea salts and biogenic components (Wang and Zhang, 2001; Zhang Y. et al., 2019). Through either direct (Coakley et al., 1983; Jacobson, 2001; Bond et al., 2013; Li et al., 2017) or indirect effects on atmospheric radiation (Charlson et al., 1992; Guo et al., 2018; Liu et al., 2021), aerosols are well recognized to significantly influence weather and climate at regional and global scales (Menon et al., 2002; Lau et al., 2006; Zhang et al., 2007; Tosca et al., 2010; Bollasina et al., 2011; Li et al., 2011; Wang et al., 2011, 2013; Hwang et al., 2013; Wu et al., 2016a; Zhang et al., 2021). Aerosols can also cause serious environmental problems such as fog, haze, photochemical smog and acid rain, with significant impacts on the hydrological cycle, new energy development, agricultural production and transportation (Ramanathan et al., 2001; Haywood et al., 2011; Singh et al., 2017; Sweerts et al., 2019). Fine particulate matter with particle diameters less than 2.5 μm, commonly termed $PM_{2.5}$, are generally thought of as one of the main causes of air pollution and have an adverse effect on human health. According to the Global Burden of Disease 2010 comparative risk assessment (GBD, Lim et al., 2012), roughly 3.2 million deaths per year are attributable to ambient $PM_{2.5}$. Understanding and predicting $PM_{2.5}$ and its spatial and temporal variations are therefore vital for reducing mortality and other impacts on the environment (Apte et al., 2015).

With the development of Earth System Models (ESMs), the importance of coupling between multiple components of the Earth System, including atmosphere, ocean, land and sea ice, has gradually been recognized, and increasingly improved

within these ESMs. ESMs have become an important tool to simulate and forecast global aerosols (Collins et al., 2017) and can not only fill the gaps between historical observations, but also estimate the trends of aerosols in the future, and thus provide a basis for assessing the evolution of air pollution in both the past and future. The performance of ESMs to reproduce the observed aerosols is an important issue for climate modelling communities. In fact, the Atmospheric Chemistry and Climate Model Intercomparison Project (ACCMIP) was endorsed by the Fifth Coupled Model Intercomparison Project Phase 5 (CMIP5), and tended to focus on the atmospheric chemistry (Lamarque et al., 2013), with only a few models providing the simulation results for aerosols (Collins et al., 2017). The Aerosols and Chemistry Model Intercomparison Project (AerChemMIP, Collins et al., 2017), part of the Sixth Coupled Model Intercomparison Project Phase 6 (CMIP6, Eyring et al., 2016), provides an opportunity to understand the performance of the latest ESMs in simulating aerosols. There are few relevant assessments on the performance of CMIP6 ESMs in simulating aerosols (Mulcahy et al., 2020; Wu et al., 2020). They show that most of the current generation of ESMs such as BCC-ESM1 and UKESM1 can reproduce the global spatial distributions of most aerosol components (e.g., sulfate) concentrations, although there are some model biases for certain components.

It is important to understand the evolution of ground-level $PM_{2.5}$ over Asia as it is one of the most heavily polluted regions on the globe, and has the highest mortality rate attributed to atmospheric pollution (Apte et al., 2015). Previous studies show that most of the CMIP6 ESMs can capture the spatial distributions of surface $PM_{2.5}$ concentrations across the globe but underestimate the absolute magnitude (Turnock et al., 2020). **However, the ability of the CMIP6 ESMs to simulate $PM_{2.5}$ in Asia has not been carefully explored so far largely due to the lack of ground-based surface**

aerosol observations in Asia. In addition, the various components of $PM_{2.5}$ have seldom been utilized in previous studies, leading to the differences among models being poorly understood.

Here, simulations of surface $PM_{2.5}$ and its component concentrations from ten CMIP6 ESMs are evaluated in detail against observations from surface sites over Asia. Based on the ratio of $PM_{2.5}$ to main aerosol mass and the relative contributions of each component to $PM_{2.5}$, differences among models are revealed. The remaining parts of this manuscript are as follows: the research data and methods are presented in section 2; in section 3, we assess the ability of the CMIP6 ESMs to simulate the spatial distribution of $PM_{2.5}$ and its main components in Asia; in section 4, we analyze their model-spread among 10 ESMs; uncertainties in evaluating $PM_{2.5}$ concentrations is discussed in section 5; a summary is given in section 6.

2. Data and Methods

The monthly mean $PM_{2.5}$ components, including sulfate, organic aerosol (OA), black carbon (BC), dust, and sea salt, from ten ESMs participated in CMIP6 are employed in this study. The model information is described in Table 1 and all the model data can be freely download from the Earth System Grid Federation (ESGF) nodes (https://esgf-node.llnl.gov/search/cmip6/, last access: 10 January 2022). All the models use the same anthropogenic emission inventory from the Community Emissions Data System (CEDS, Hoesly et al., 2018, http://www.globalchange.umd.edu/ceds/ceds-cmip6-data/) and their own schemes for simulating natural emissions such as dust and sea salt aerosols, which have different representations of the aerosol size distribution (Collins et al., 2017). The model data is obtained from the CMIP6 historical

138 experiments (Eyring et al., 2016) before 2015 and from the SSP370 experiments in
139 AerChemMIP (Collins et al., 2017) afterward.

140

141 **Table1.** CMIP6 Earth system models used in this study

CMIP6 ESMs	Institution	Resolution and Vert levels in Atmosphere	Aerosol Component Name and References	Natural aerosols size bins (μm)	Model and Data References
BCC-ESM1	Beijing Climate Center, China Meteorological Administration, China	2.813° × 2.813°; L26; top level at 2.91hPa.	BCC-AGCM3-Chem, Wu et al., 2020.	Dust (4 size bins: 0.1–1, 1–2.5, 2.5–5, 5–10μm); Sea salt (4 size bins: 0.2–1, 1–3, 3–10, 10–20μm)	Wu et al., 2020; Zhang et al., 2018, 2019a
CESM2-WACCM	National Center for Atmospheric Research, United States	0.9° × 1.25°; L70; top level at $6x10^{-6}$ hPa.	MAM4, Liu et al., 2016.	Dust and sea salt (log-normal size distribution)	Danabasoglu et al., 2020; Danabasoglu, 2019a, 2019b
EC-Earth3-AerChem	European consortium of meteorological services, research institutes, and high-performance computing centers	3°× 2°; L34; top level: 0.1 hPa.	TM5, Krol et al., 2005; Huijnen et al., 2010.	Dust and sea salt (7 size bins, log-normal size distributions)	Van Noije et al., 2021; EC-Earth Consortium, 2020a, 2020b
GFDL-ESM4	NOAA Geophysical Fluid Dynamics Laboratory, United States	Cubed-sphere (c96) grid, with ~100 km native resolution, regridded to 1.0° × 1.25°; L49; top level at 0.01 hPa.	GFDL AM4.1, Horowitz et al., 2020.	Dust (5 size bins: 0.1–2, 2–4, 4–6, 6–12, 12-20μm); Sea salt (5 size bins)	Dunne et al., 2020; John et al., 2018; Krasting et al., 2018
IPSL-CM5A2-INCA	Institut Pierre Simon Laplace, Paris, France	3.75°× 1.875°; L39； top level 80km.	INCA v6 NMHC-AER-S	Dust and sea salt particles are partitioned into 3 size classes (< 1 μm, 1-10μm, >10 μm), Szopa et al., 2013	Sepulchre et al., 2020; Boucher et al., 2020a, 2020b
MIROC-ES2L	University of Tokyo, National Institute for Environmental Studies, and Japan Agency for Marine-Earth Science and Technology, Japan	2.813° × 2.813°; L40; top level at 3.0 hPa.	SPRINTARS, Takemura et al., 2000, 2005, 2009.	Dust (10 size bins: from 0.1 to 10 μm); Sea salt (10 size bins: from 0.05 to 10 μm, lognormal distribution)	Hajima et al., 2020; Hajima et al., 2019; Tachiiri et al., 2019
MPI-ESM-1-2-HAM	Max Planck Institute for Meteorology, Germany	1.875° × 1.875°; L47; top level at 0.01 hPa.	HAM2.3, Tegen et al., 2019.	Dust and sea salt size distribution is represented by 7 lognormal modes	Neubauer et al., 2019a, 2019b
MRI-ESM2-0	Meteorological Research Institute, Japan	1.125° × 1.125°; L80; top level at 0.01 hpa.	MASINGAR mk-2r4c, Yukimoto et al., 2019a; Oshima et al., 2020.	Dust and sea salt (10 size bins: from 0.1 to 10 μm)	Yukimoto et al., 2019a; Yukimoto et al., 2019b, 2019c
NorESM2-LM	Norwegian Climate Center, Norway	1.9° × 2.5°; L32; top level at 3.64 hPa.	OsloAero6, Kirkeväg et al., 2018; Seland et al., 2020.	Dust and sea salt, lognormal distribution	Kirkeväg et al., 2018; Seland et al., 2019a, 2019b
UKESM1-0-LL	Natural Environment Research Council, and Met office, United Kingdom	1.25° × 1.875°; L85; top level at 85km.	GLOMAP-Mode, Mulcahy et al., 2020.	Dust (6 size bins); Sea salt (5 size bins)	Sellar et al., 2019; Good et al., 2019; Tang et al., 2019

142

Not all CMIP6 ESMs provide $PM_{2.5}$ concentrations, even for some ESMs with available $PM_{2.5}$, they use different methods to calculate it. In order to uniformly evaluate the ability of ESMs to simulate $PM_{2.5}$, it is necessary to find a consistent method to calculate $PM_{2.5}$. Therefore, following the methods used in other studies (Silva et al., 2013; Turnock et al., 2020), the formula used to estimate $PM_{2.5}$ mass concentrations from the ESMs data is expressed as

$$PM_{2.5} = BC + OA + SO_4 + (0.1 \times DU) + (0.25 \times SS)\,, \quad (1)$$

where BC, OA, SO_4, DU, SS represent the black carbon (CMIP6 diagnostic identifier: mmrbc), organic aerosol (mmroa), sulfate (mmrso4), dust (mmrdust) and sea salt (mmrss) mass mixing ratio (kg kg^{-1}), respectively. All the aerosol mass concentrations in the lowest layer of each ESM are taken as the near surface values from simulations in this work. The particles for BC, OA and SO_4 aerosols are generally less than 2.5 μm in diameter.

In Eq. (1), 10% and 25% of dust and sea salt particles are assumed to be present within the fine size fraction of less than 2.5 μm in diameter. We validated this assumption for dust and sea salt from additional BCC-ESM1 simulations which provided output across four-size bins of dust (DST01: 0.1-1.0 μm, DST02: 1.0-2.5 μm, DST03: 2.5-5.0 μm, DST04: 5.0-10 μm) and sea salt (SSLT01: 0.2-1.0 μm, SSLT02: 1.0-3.0 μm, SSLT03: 3.0-10 μm, and SSLT04: 10-20 μm) aerosols (Wu et al., 2020). Only the ESGF provides total aerosol mass mixing ratios so we only have access to full size resolved aerosol data from BCC-ESM1. As shown in Figure 1, the estimated $PM_{2.5}$ fine particles concentrations for dust (hereafter $PM_{2.5}$DU) and sea salt ($PM_{2.5}$SS) from the Eq. (1) are nearly consistent to that from the original BCC-ESM1 simulations (fine size fraction less than 2.5 μm in diameter calculated by summing by DST01 and DST02, SSLT01 and SSLT02, respectively).

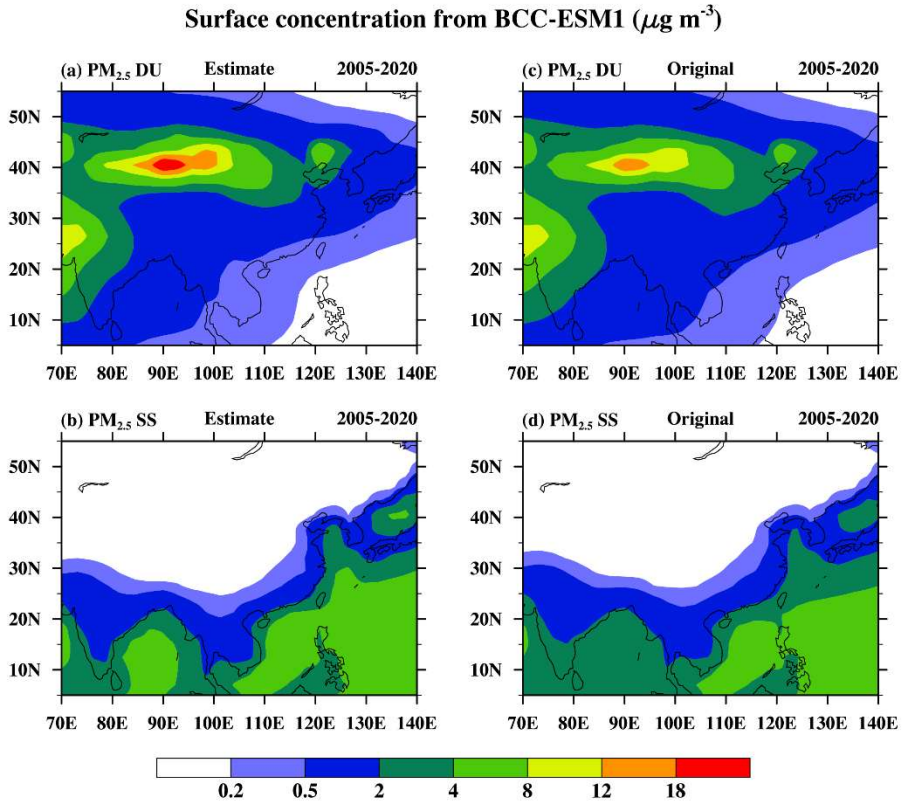

168

169 **Fig. 1.** Annual mean of near surface $PM_{2.5}$DU and $PM_{2.5}$SS concentrations in Asia (70–140° E, 5–55° N)
170 during 2005–2020 from BCC-ESM1 simulations. (a) and (b) denotes the estimated values by Eq. (1) for
171 $PM_{2.5}$DU and $PM_{2.5}$SS, respectively. (c) and (d) show the original model data for total of dust and sea
172 salt with fine size fraction less than 2.5 μm in diameter. Units: $\mu g \cdot m^{-3}$.

173

174 To evaluate the present-day $PM_{2.5}$ climatology in ESMs, the following ground-
175 based observations are used: monthly mean surface $PM_{2.5}$ observations during 2014–
176 2019 at 25 sites in Asia from the Acid Deposition Monitoring Network in East Asia
177 (hereafter EANET data, http://www.eanet.asia, last access: 16 December 2020) and 348
178 urban sites in China available from the Chinese National Environmental Monitoring
179 Center (hereafter CNEMC data, http://www.cnemc.cn, last access: 16 December 2020).
180 The CNEMC data have been used in previous studies (Wei et al., 2019; Wei et al.,
181 2020). In order to examine the observation uncertainty due to the impact of urban
182 effects, monthly mean $PM_{2.5}$ concentrations at two atmospheric background stations

183 from the Meteorological Observation Center, China Meteorological Administration
184 (hereafter CMA data, Zhang et al., 2020) are compared with the nearby urban sites from
185 CNEMC data, as well as from a pair of urban and suburban ground-based observations
186 in Thailand (Pathumwan and KlongHa) from the Asia-Pacific Aerosol Database
187 (APAD, Cohen and Atanacio, 2015). The geographic distributions of all the observation
188 sites and division of Asian subregions used in the study are shown in Figure 2.

189 Considering the sparsely covered and unevenly distributed ground-based
190 observation, the Modern-Era Retrospective Analysis for Research and Applications,
191 version 2 (MERRA-2) data, a high-resolution ($0.5^{o}\times0.625^{o}$) assimilation data product
192 (including sulfate, organic aerosols, black carbon, dust and sea salt) developed by
193 combining satellite observations with the Goddard Earth Observing System
194 atmospheric model and atmosphere data assimilation system (Buchard et al., 2016;
195 Randles et al., 2017) is further used. The MERRA-2 data is widely used by many
196 studies in evaluation of aerosols simulations (Turnock et al., 2020; Ukhov et al., 2020;
197 Li et al., 2021; Zhao et al., 2021). For inter-comparison between ESMs and MERRA-
198 2, we derive the monthly MERRA-2 $PM_{2.5}$ data from 2005 to 2020 using the same
199 equation (1), on the basis of the monthly sulfate, organic aerosols, black carbon, and
200 total mass of dust and sea salt aerosols mass data that are directly downloaded from the
201 website (https://gmao.gsfc.nasa.gov/reanalysis/MERRA-2/data_access/, last access: 16
202 December 2020). In this study, all model data were interpolated to the same horizontal
203 resolution of 0.5°×0.625° latitude/longitude grids as in MERRA-2, and onto the site
204 locations when compared with the ground-based observations.

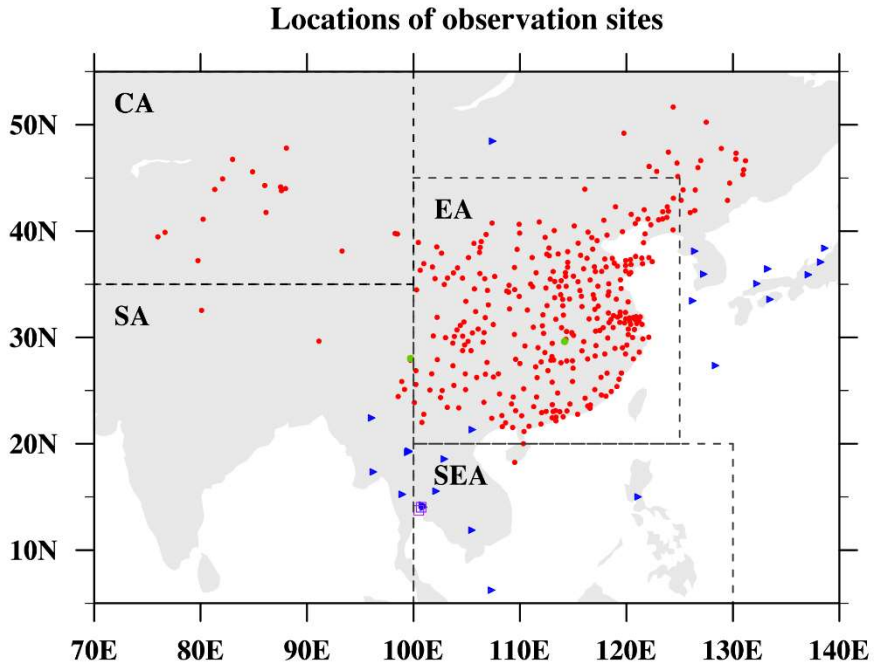

Fig. 2. Locations of observation sites in Asia (70–140° E, 5–55° N) from EANET (blue triangles, 25 sites), CNEMC (red circles, 348 urban sites), CMA (green circles, 2 background stations) and APAD (purple hollow squares, 2 adjacent sites). The dashed areas represent the various parts of Asia, including Central Asia (CA), East Asia (EA), South Asia (SA) and Southeast Asia (SEA).

3. The present-day climate of $PM_{2.5}$ and its components in Asia

3.1 $PM_{2.5}$ concentrations

In this section, we will focus on the spatial features of present-day climate mean $PM_{2.5}$ from 2005 to 2020. Figure 3 shows the percentage contribution of $PM_{2.5}$ to the total aerosol (fine and coarse) concentration in Asia, including sulfate, OA, BC, and all particle sizes of dust and sea salt. The results from MERRA-2 (Fig. 3l) shows a relatively high proportion of $PM_{2.5}$ over East Asia and Southeast Asia and the contribution is up to 60%–80% over the southeastern coast of China. Central Asia is an arid or semi-arid region and has the lowest proportion (less than 30%) of $PM_{2.5}$, where

221 mineral dust is generally the main source of aerosols, and coarse particles dominate.
222 For the multi-model mean (MME, Fig. 3k), the $PM_{2.5}$ ratio is in overall a good
223 agreement with MERRA-2, except for MIROC-ES2L (Fig. 3f). MIROC-ES2L shows
224 the largest proportion of fine particulate matter in eastern China, which is about 20%
225 higher than in MME and MERRA-2.
226

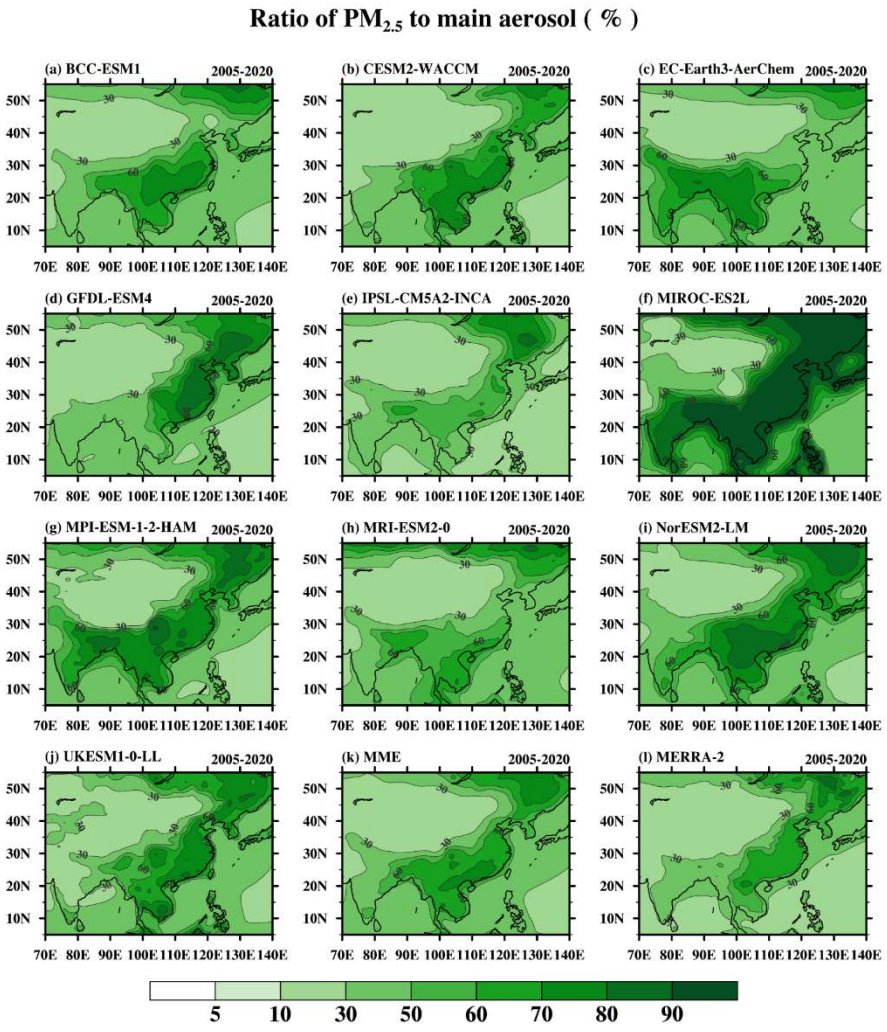

227

228 **Fig. 3.** The 2005–2020 mean $PM_{2.5}$ ratios to main aerosol (including all particle sizes of dust and sea salt,
229 sulfate, organic aerosol and black carbon) in Asia (70–140° E, 5–55° N) for (a-j) the 10 ESMs, (k) their
230 MME, and (l) MERRA-2. Units: %.

231 Figure 4a shows the spatial distribution of present-day mean of surface $PM_{2.5}$
232 concentrations in the 373 ground-based observations from CNEMC and EANET,

233 averaged for the period of 2014-2019. Annual mean surface $PM_{2.5}$ concentrations in
234 most parts of eastern China can be over 40 μg m^{-3}, and the highest values are mainly
235 centered over the Beijing-Tianjin-Hebei region where $PM_{2.5}$ concentration may be over
236 60 μg m^{-3}. High annual mean $PM_{2.5}$ concentrations are also present over northwestern
237 China, mainly contributed by mineral dust. In the area south of 25°N, the annual mean
238 $PM_{2.5}$ concentrations are generally smaller, which may be caused by strong wet
239 deposition and lower emissions. Japan and Korea are also regions with values of annual
240 mean $PM_{2.5}$ concentrations less than 20 μg m^{-3}. Figures 4b-4k show the point-to-point
241 comparisons between ten ESMs simulations separately with 373 ground-based
242 observations in the same period from 2014 to 2019. They illustrate that most models
243 underestimate the observations, although all ESMs show high spatial correlations of
244 0.52 to 0.74 and 0.69 for MME (Fig. 4l). The underestimation of $PM_{2.5}$ concentrations
245 by CMIP6 models in this study partly comes from the use of the approximate method
246 to calculate $PM_{2.5}$ (Equation (1)), in which nitrate (NO_3^-) and ammonium (NH_4^+)
247 aerosols are not involved. Those underestimations also exist in CMIP5 models (Wu et
248 al., 2016b; Liu et al., 2017).

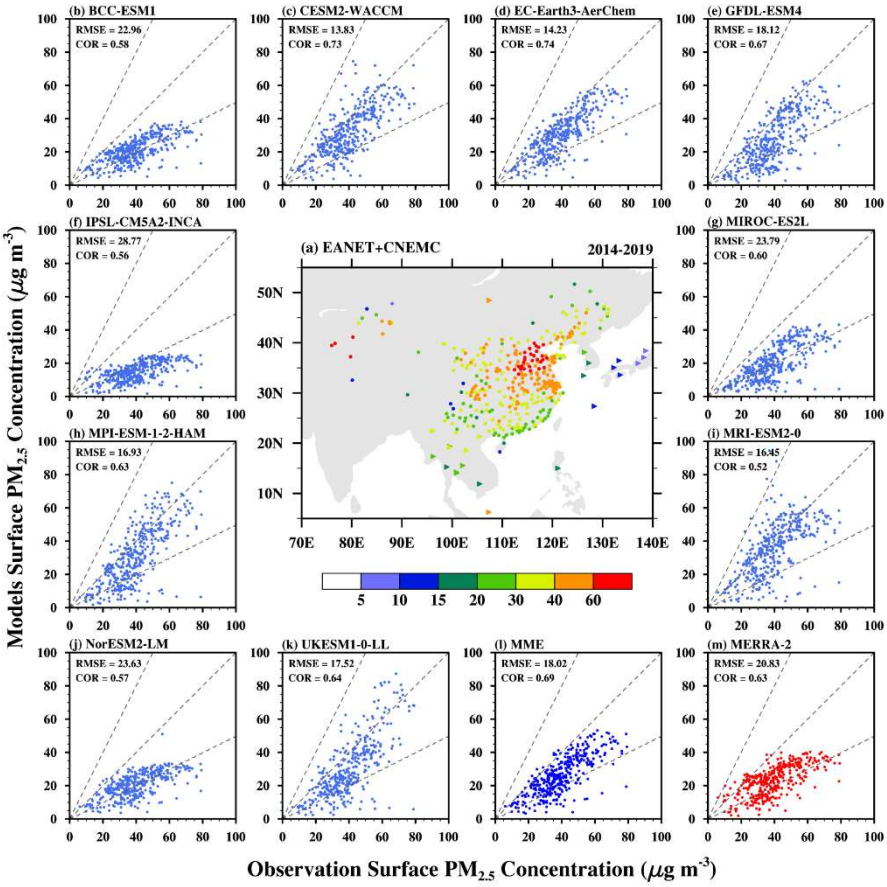

Fig. 4. (a) 2014–2019 averaged annual mean surface $PM_{2.5}$ concentrations for 373 sites from EANET (triangles, 25 sites) and CNEMC (circles, 348 urban sites) in Asia. (b-m) Scatterplots of surface $PM_{2.5}$ concentrations for each ESMs and their MME, and MERRA-2, separately comparing to the observations from EANET and CNEMC sites during the same period. RMSE stands for root-mean-square error, and COR for correlation coefficient. The grey lines represent the 1:1 line, 1:2 line and 2:1 line, respectively. Units: μg m^{-3}.

As shown in Figure 4m, the MERRA-2 data also underestimate the observed $PM_{2.5}$ concentrations at 373 sites. Nevertheless, MERRA-2 can provide the overall spatial distribution of $PM_{2.5}$ in Asia with better temporal and spatial coverage and compensate for the gaps not covered by site observations. As shown in Fig. 5l, the spatial distribution of annual mean surface $PM_{2.5}$ concentrations averaged for 2005 to 2020 from MERRA-2 is similar to that from ground-based observations (Fig. 4a). Except for the two regions with high surface $PM_{2.5}$ concentrations in eastern China and

264 northwestern China that can be found from ground-based observations, MERRA-2 (Fig.
265 5l) also shows a third region of high-concentration centered in northern India where
266 there are high local emissions and where the Himalayas plays a large role in preventing
267 dispersal of aerosols (Shi et al., 2018). The $PM_{2.5}$ concentrations are less than 5μg m^{-3}
268 over the Tibetan Plateau (about 73–104° E, 26–39° N) and Mongolia Plateau (about 87–
269 122° E, 37–53° N), where human activities are weak.
270

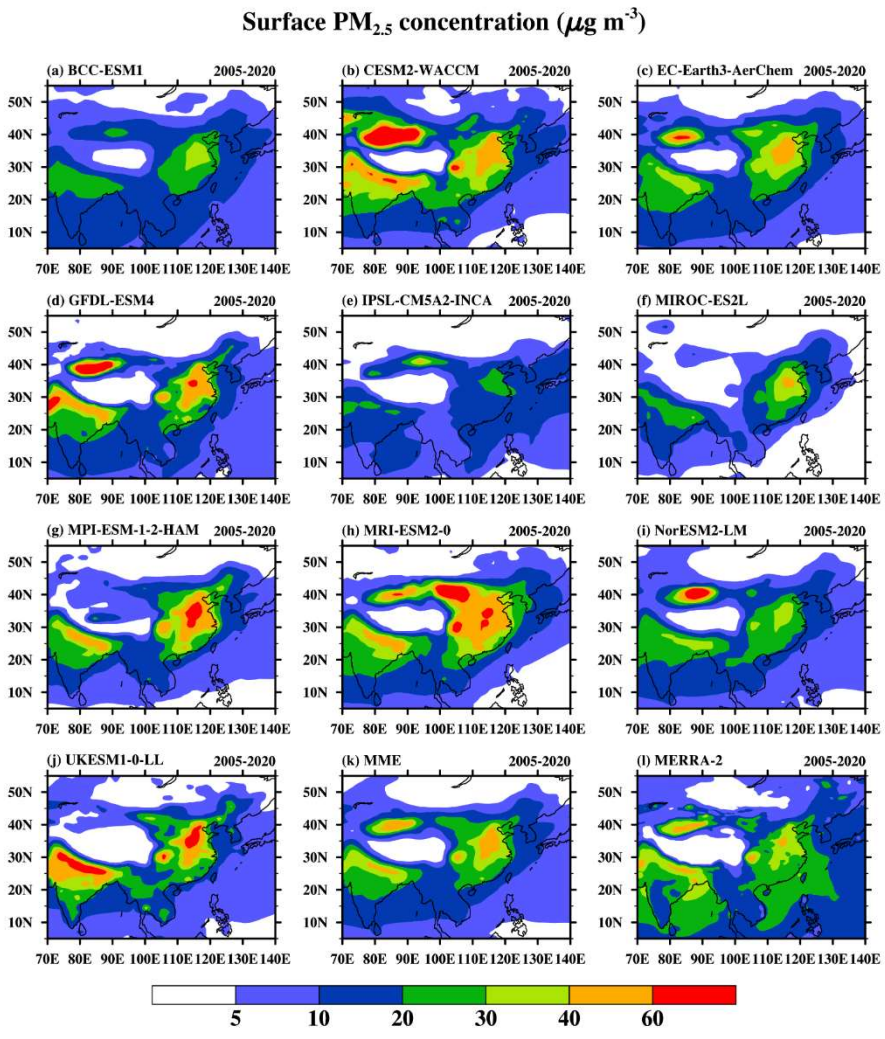

271

272 **Fig. 5.** 2005–2020 averaged annual mean surface $PM_{2.5}$ concentrations in Asia (70–140° E, 5–55° N)
273 from (a-j) 10 ESMs, (k) their MME, and (l) MERRA-2. Units: μg m^{-3}.

274 The main spatial features of surface $PM_{2.5}$ concentrations are generally well
275 captured by the ESMs (Fig. 5a-k) in comparison with MERRA-2 (Fig. 5l), except over

the offshore area where MERRA-2 data overestimated sea salt as pointed out in Buchard et al. (2017). However, there exists a large diversity among models, especially over the three $PM_{2.5}$ centers (eastern China, northern India, and in the northwestern China and Mongolia, Fig. 6a). The amplitude of model-spread (that is denoted by the standard deviation of simulated $PM_{2.5}$ concentration among 10 ESMs in the study) over the northwestern China and Mongolia are close to the MME regional $PM_{2.5}$ concentration (Fig. 6b). Specifically, CESM2-WACCM (Fig. 5b) overestimates $PM_{2.5}$ in Taklimakan desert of central Xinjiang (> 60μg m^{-3}), and MRI-ESM2-0 (Fig. 5h) has an abnormally high-value center in the Mongolian plateau. The dominant species of $PM_{2.5}$ vary with regions as well as the one responsible for the model-spread in $PM_{2.5}$ simulation, which will be discussed in detail in section 4.

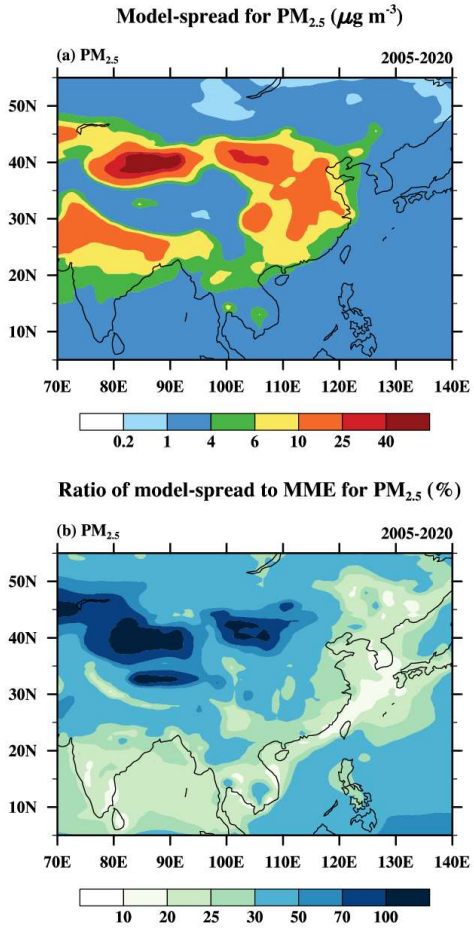

289 **Fig. 6.** The model-spread (units: μg m^{-3}) among the 10 ESMs and the ratio (units: %) of model-spread to
290 MME for annual mean of surface $PM_{2.5}$ concentration during 2005-2020.
291

292 ***3.2 The main components of $PM_{2.5}$ concentrations***

293 Sulfate, OA, and BC are the main $PM_{2.5}$ aerosols from anthropogenic emissions
294 in Asia and are the main $PM_{2.5}$ species over eastern China and northern India (Fig. 7-
295 9). In MERRA-2, sulfate (Fig. 7l) and BC (Fig. 9l) concentrations in eastern China are
296 higher than those in northern India, whereas the spatial distribution for OA shows the
297 opposite (Fig. 8l). The MME can generally reproduce the spatial distribution for sulfate
298 (Fig. 7k), OA (Fig. 8k), and BC (Fig. 9k) although their magnitudes are underestimated
299 for sulfate but overestimated for OA and BC. There are significant differences in the
300 simulations of sulfate and OA among various ESMs. MRI-ESM2-0 (Fig. 7h) has the
301 highest concentration of sulfate in southeastern China, while IPSL-CM5A2-INCA (Fig.
302 7e) has the lowest sulfate concentrations. CESM2-WACCM (Fig. 8b) and UKESM1-
303 0-LL (Fig. 8j) have larger concentrations of OA than other ESMs, which may be caused
304 by different volatile organic compounds (VOC) and secondary organic aerosol (SOA)
305 formation mechanisms in the ESMs. UKESM1-0-LL also shows the largest BC
306 concentration than the others (Fig. 9j).
307

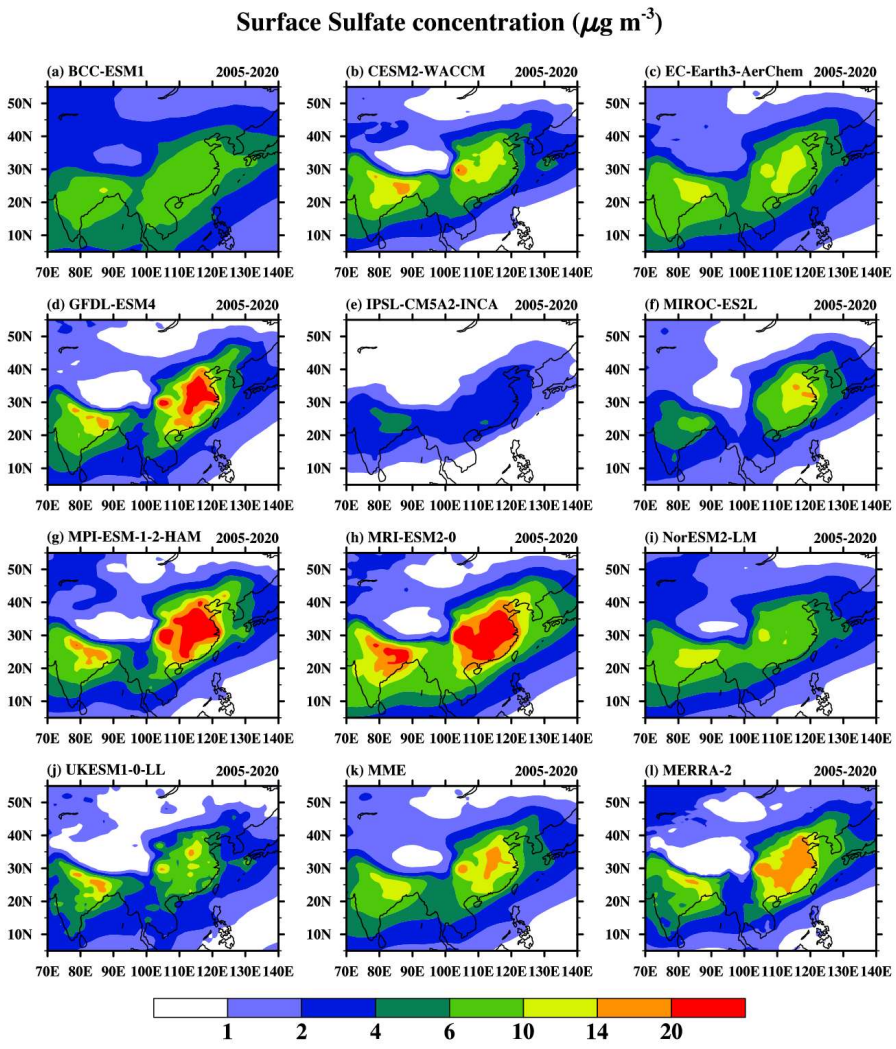

308

309 **Fig. 7.** The same as in Fig. 5, but for the sulfate.

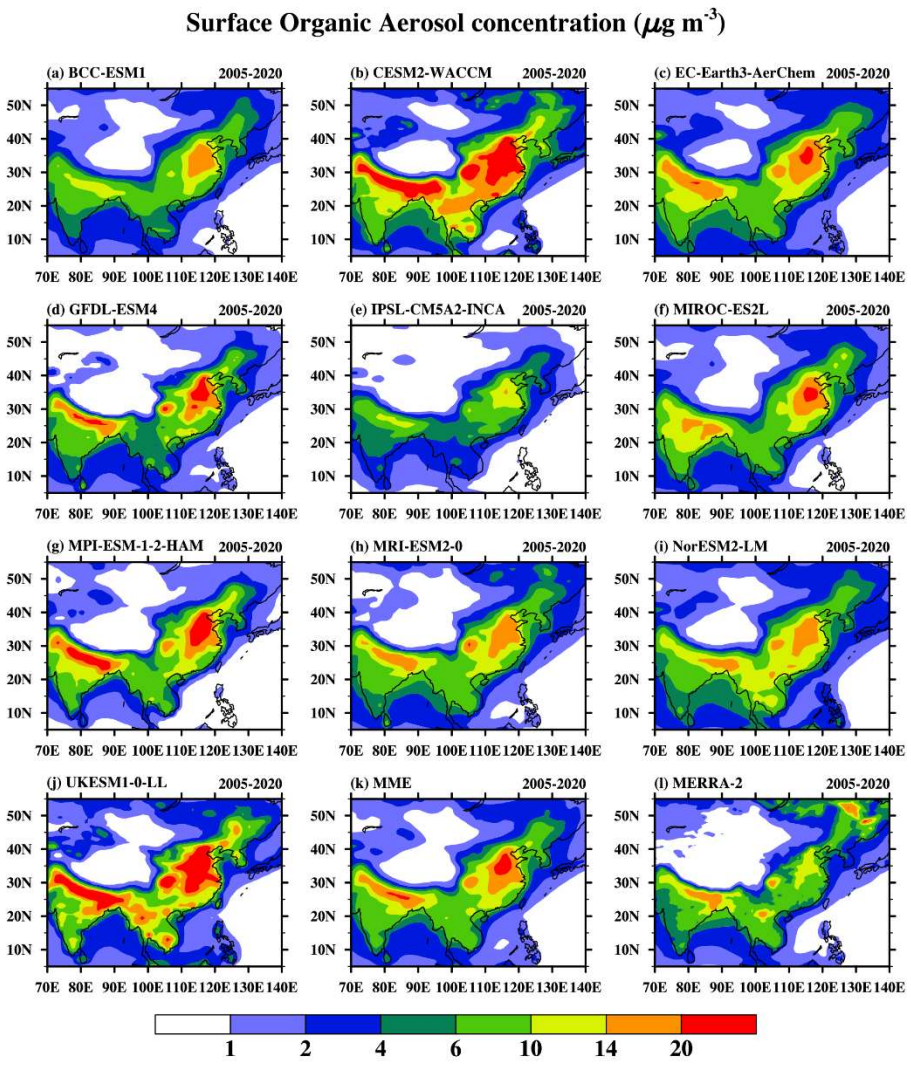

310

311 **Fig. 8.** The same as in Fig. 5, but for the organic aerosol.

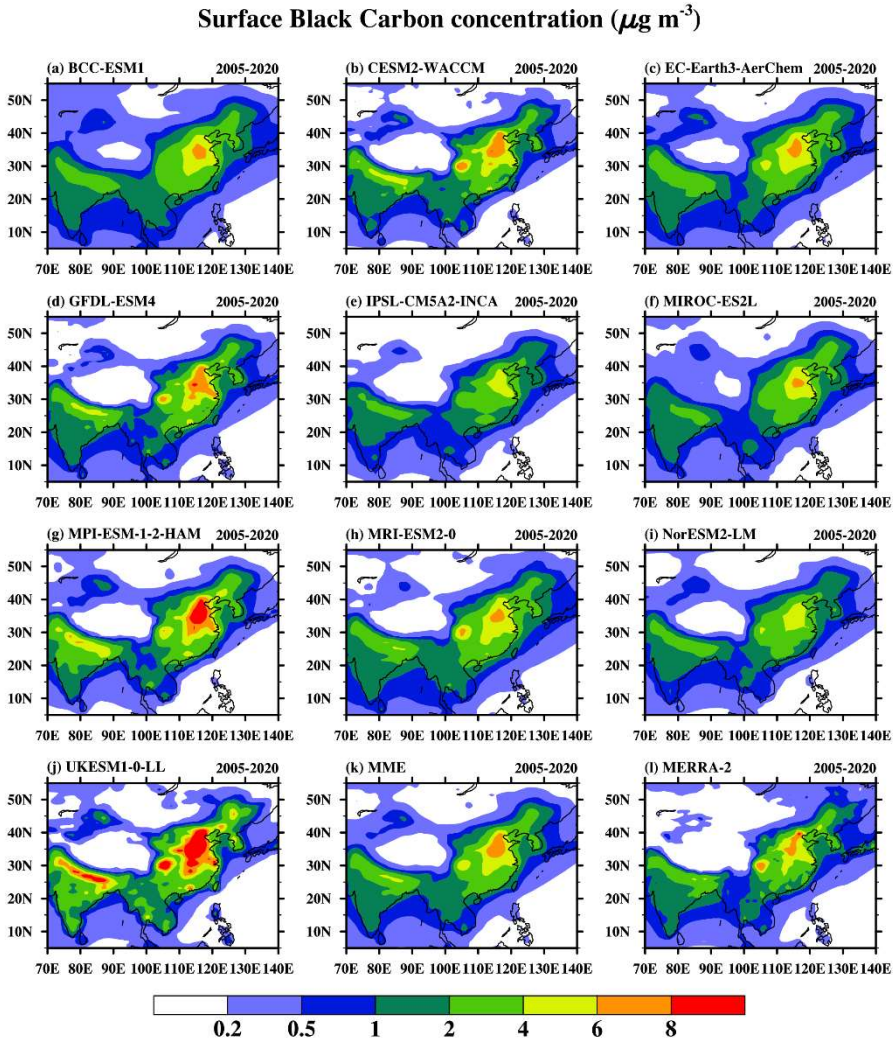

312

313 **Fig. 9.** The same as in Fig. 5, but for the black carbon.

314 $PM_{2.5}$DU and $PM_{2.5}$SS are the natural components in $PM_{2.5}$. As shown in Fig.
315 10, $PM_{2.5}$DU is responsible for the $PM_{2.5}$ center (Fig. 5) over the northwestern China
316 and Mongolia. The $PM_{2.5}$DU concentrations from MME (Fig. 10k) is similar to that
317 from MERRA-2 (Fig. 10l). But there are large differences in $PM_{2.5}$DU simulations
318 among 10 ESMs. CESM2-WACCM (Fig. 10b) and GFDL-ESM4 (Fig. 10d) simulated
319 larger $PM_{2.5}$DU concentrations than other models. And the $PM_{2.5}$DU in MIROC-ES2L
320 (Fig. 10f) is much smaller than MERRA-2 (Fig. 10l), with $PM_{2.5}$DU differences up to
321 20 μg m^{-3}. In MRI-ESM2-0 (Fig. 10h), the high $PM_{2.5}$DU center extends eastward to
322 north China and the amplitude of $PM_{2.5}$DU is about twice of that in the east, which is

not evident in MERRA-2 (Fig. 10l). In addition, MPI-ESM-1-2-HAM (Fig. 10g) simulated excessive amount of $PM_{2.5}$DU in northern part of Tibetan plateau, which is distinctive from other models. $PM_{2.5}$SS is another important natural aerosol mainly distributed over oceans and coastal regions. The $PM_{2.5}$SS concentration over land is lower than the other species in $PM_{2.5}$, and the differences among ESMs are generally small (Fig. 11). Due to the known overestimation of sea salt in MERRA-2 (Buchard et al., 2017), there are significant differences between the MME and MERRA-2 (Fig. 11k and Fig. 11l).

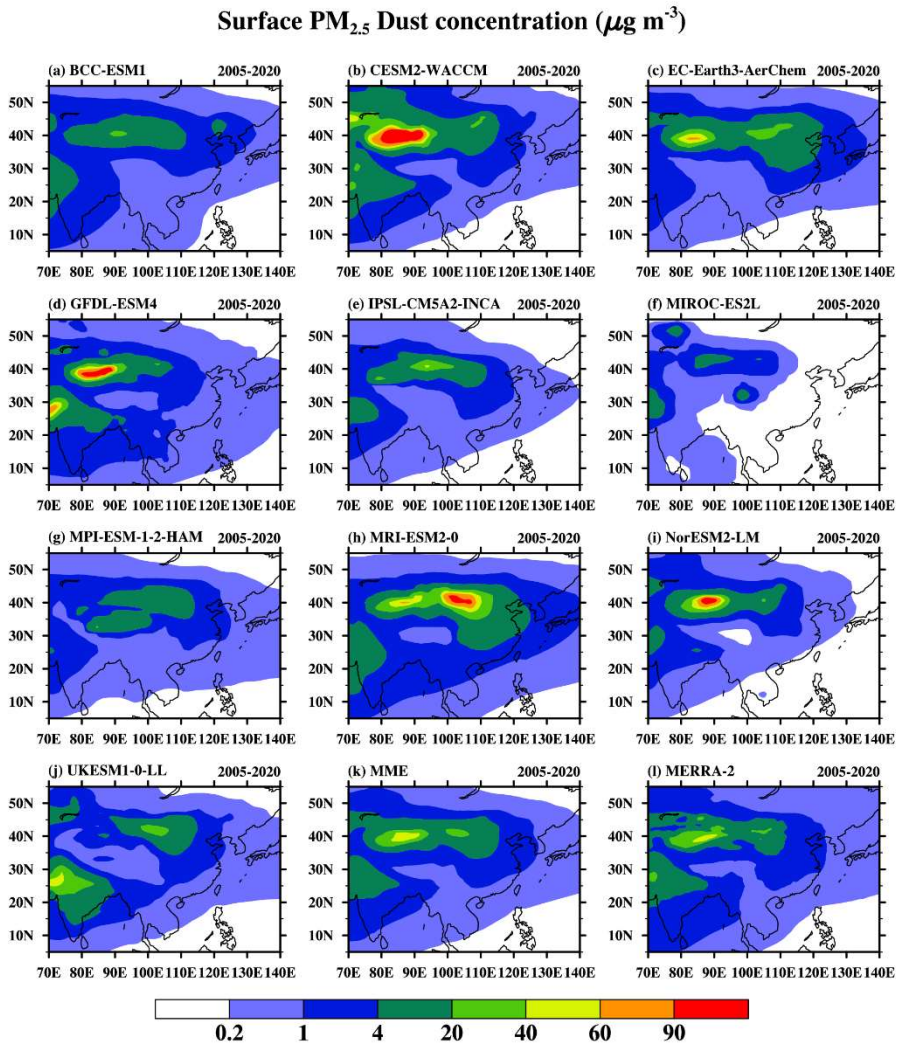

Fig. 10. The same as in Fig. 5, but for the $PM_{2.5}$ fine particles of dust.

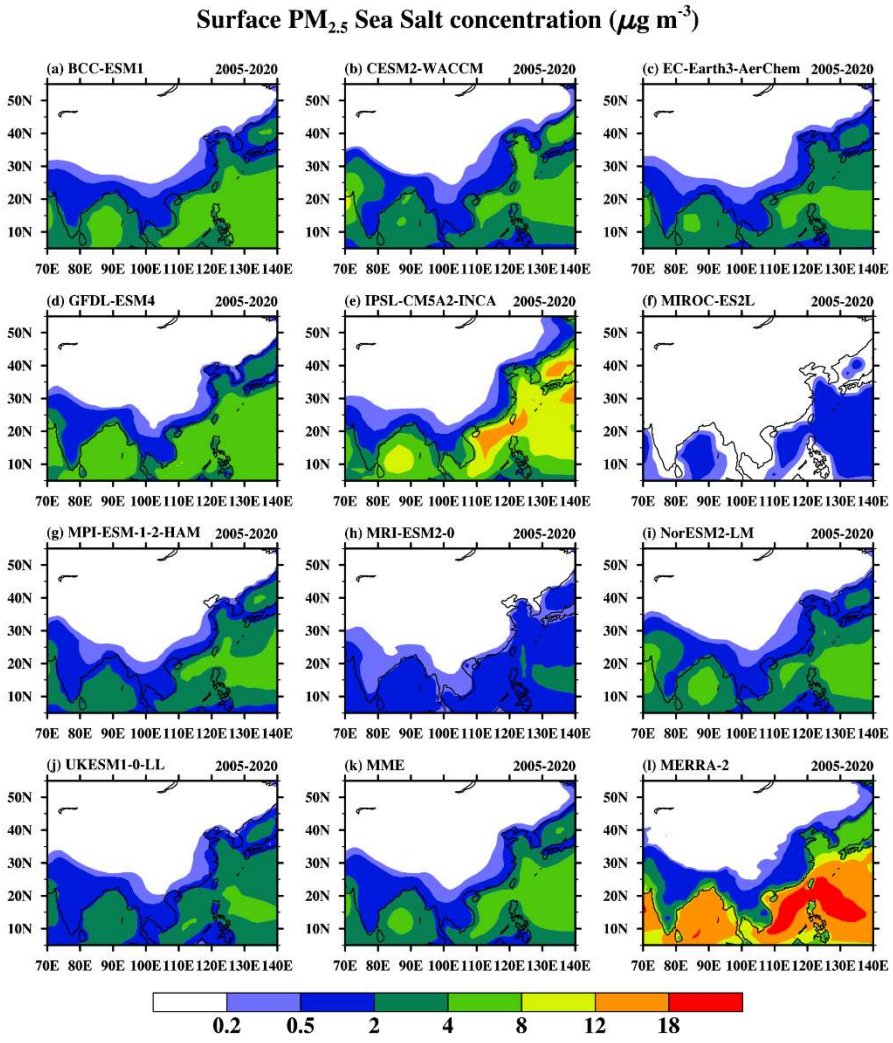

333

334 **Fig. 11.** The same as in Fig. 5, but for the $PM_{2.5}$ fine particles of sea salt.

335

336 # 4. Uncertainties in simulated $PM_{2.5}$ concentrations from

337 # ESMs

338 ## *4.1 The uncertainty in the anthropogenic and natural $PM_{2.5}$ species*

339 Figure 12 shows the model-spread among ten ESMs for main anthropogenic

340 components of $PM_{2.5}$, sulfate, OA, and BC. The regions of large model-spread are

341 evident over eastern China, northern India, and Sichuan Basin, the main anthropogenic

342 emission centers in Asia. All the ESMs used the same anthropogenic emissions

343 inventory (Hoesly et al., 2018). Large model-spread for anthropogenic aerosols in
344 individual ESMs thus mainly comes from the different way that individual models
345 represent chemical and physical processes relevant for aerosols including dynamic
346 transport, dry deposition, gravitational settling, wet scavenging by clouds and
347 precipitation, and even their chemical processes (Textor, et al., 2007; Wu et al., 2020).
348 For example, the sulfate (Fig. 12a) uncertainty is generally larger over eastern China
349 and the Sichuan Basin than over northern India, which probably results from different
350 gas-phase and aqueous-phase conversion from SO_2 except for the above reasons. Large
351 uncertainty over the Sichuan Basin is also caused by unique topography (Liu et al.,
352 2021). The BC (Fig. 12c) uncertainty is relatively weaker as the results are mainly
353 determined by the prescribed anthropogenic emissions. For OA (Fig. 12b), the
354 concentration differences also may be caused by the way that models represent various
355 natural biogenic VOC (SOA precursors) emissions.

356 Natural aerosols are important sources of uncertainty in $PM_{2.5}$ simulation among
357 ESMs. The $PM_{2.5}$DU uncertainty prevails over the northwestern China and Mongolia,
358 the Mongolian plateau, and the Northwestern part of Indian Peninsula (Fig. 13a). There
359 are many reasons for the significant model-spread in dust simulations. In addition to
360 the effects of dynamic transport, and wet and dry depositions, large model-spread is
361 mainly caused by the difference in driving mechanisms of dust emissions that depend
362 on the meteorological drivers (winds and precipitation), especially in East China and
363 South Asia, associated with large-scale monsoonal circulations (Wilcox et al., 2020;
364 Zhao et al., 2022), the land surface conditions (Aryal et al., 2021), and the
365 representation of aerosol size distributions (Zhao et al., 2022). And the model
366 complexities also have the influence on dust concentrations (Zhao et al., 2022). As for
367 sea salt aerosols (Fig.13b), it has lower concentrations than other species, and its

368 spreads among models are less than 1 μg m^{-3} over land. Sea salt emissions are mainly
369 determined by near surface wind across the ocean (Wu et al., 2020). It is possible that
370 there is a small model-spread in surface winds across the ocean leading to less spread
371 in sea salt emissions, although inter-model differences in advective transport, and wet
372 or dry deposition will be similar to those for dust (Witek et al., 2007; Wu et al., 2020),
373 which can also affect the simulation of sea salt.
374

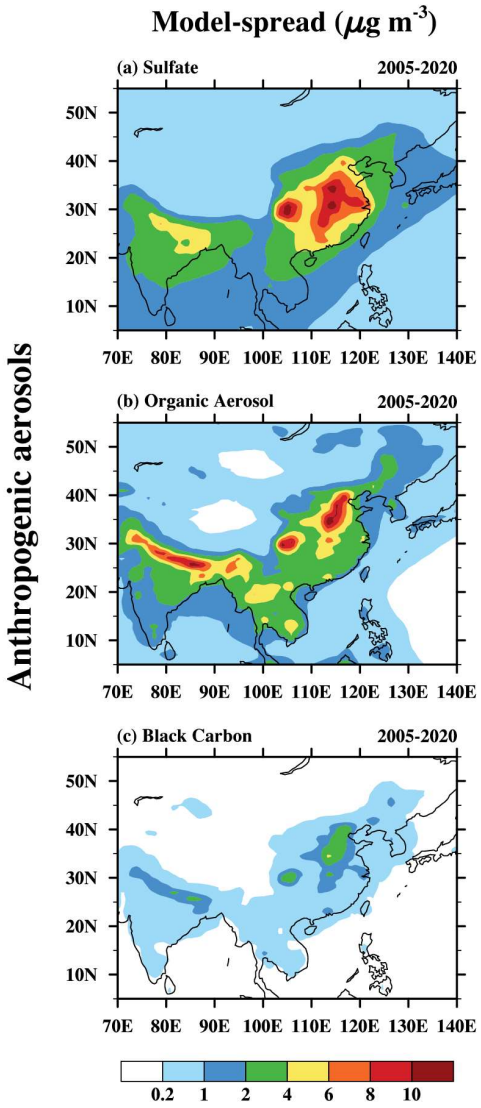

375

376 **Fig. 12.** The model-spread of annual mean concentrations for anthropogenic aerosols during 2005-2020.
377 (a) sulfate, (b) OA, and (c) BC. Units: μg m^{-3}.

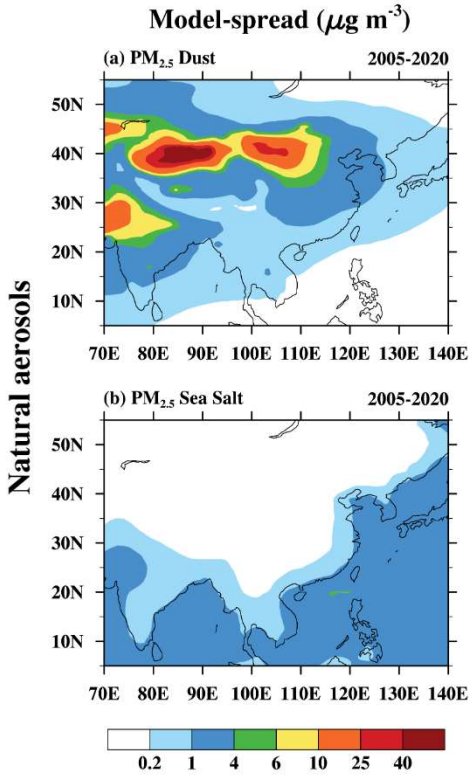

Fig. 13. The same as in Fig. 12, but for the natural aerosols. (a) $PM_{2.5}$DU and (b) $PM_{2.5}$SS. Units: μg m^{-3}.

The Taylor diagram in Figure 14 statistically examines the spatial distribution as well as the spatial variability of the differences between ESMs and MERRA-2 for main species of $PM_{2.5}$. The spatial distribution of BC concentrations simulated by ESMs are the best captured with spatial correlation coefficients of 0.9-0.97, followed by sulfate, OA, $PM_{2.5}$DU, and $PM_{2.5}$SS. For $PM_{2.5}$DU, there are large differences between the individual ESMs and MERRA-2, with normalized standard deviations ranging from 0.2 to 3.5 and spatial correlation coefficients from 0.4 to 0.87. The normalized standard deviations of CESM2-WACCM and MRI-ESM2-0 are greater than 2, indicating that the spatial variability of $PM_{2.5}$DU is largely overestimated in the two models. Although the spatial correlation coefficient of $PM_{2.5}$SS can be 0.95 or higher, the normalized standard deviations of less than 0.6 in all ESMs, resulting from the overestimation of $PM_{2.5}$SS in MERRA-2. In general, although there are differences between individual

ESMs, the MME can still capture the spatial distributions of five components from $PM_{2.5}$ well compared to MERRA-2. The spatial variations in ESMs are larger than MERRA-2 for OA, BC and $PM_{2.5}$DU.

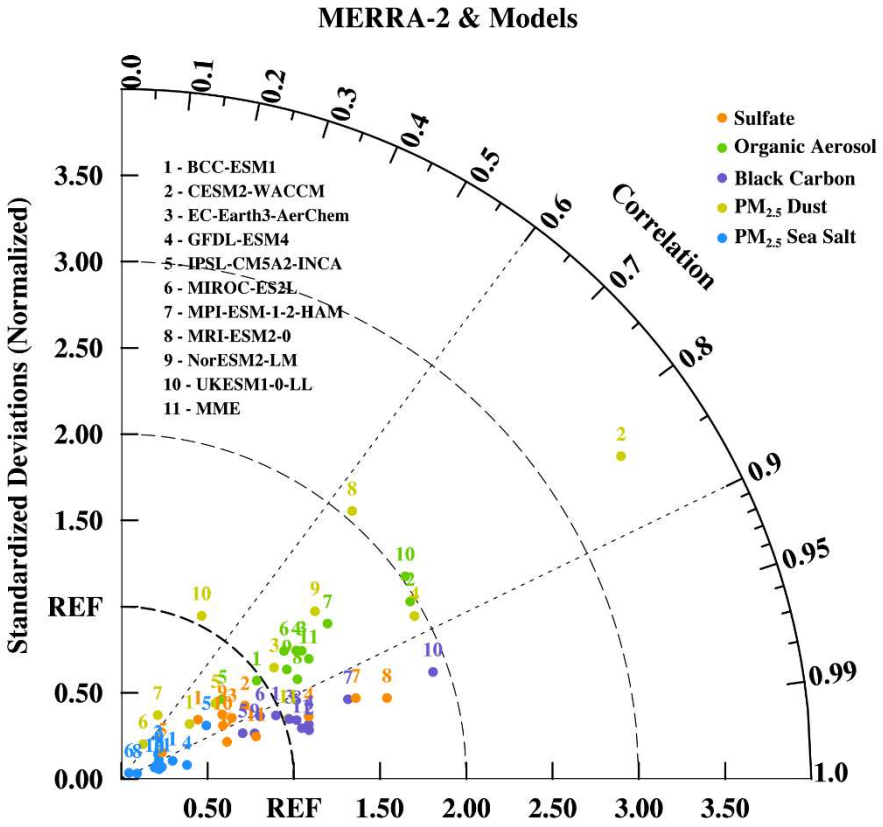

Fig. 14. Taylor diagram of the annual mean surface components (sulfate, organic aerosols, black carbon, $PM_{2.5}$DU, $PM_{2.5}$SS) concentrations simulated by the 10 ESMs compared with the MERRA-2 reanalysis data during 2005-2020 in Asia (70–140° E, 5–55° N). The radial coordinate shows the standard deviation in the spatial pattern, normalized by the observed standard deviation. The azimuthal variable shows the correlation of the modeled spatial pattern with the observed spatial pattern.

4.2 The uncertainty in dominant $PM_{2.5}$ components over different subregions

Each component of $PM_{2.5}$ has different contributions to the $PM_{2.5}$ concentrations in various regions, and the contributions vary between the individual ESMs. Here we analyzed four regions as illustrated in Fig. 2, Central Asia (CA), East Asia (EA), South Asia (SA) and Southeast Asia (SEA). In the whole Asian region (70°–140° E, 5°–55° N), the area-averaged MME $PM_{2.5}$ is smaller than for MERRA-2 (by 3.7 μg m^{-3}, Fig. 15), which is largely attributed to their difference in $PM_{2.5}$SS. The main $PM_{2.5}$ components in Asia are sulfate and OA, accounting for 28% and 32% of the $PM_{2.5}$ in the MME, respectively. $PM_{2.5}$DU is the third main $PM_{2.5}$ components in Asia, accounting for 21% of the $PM_{2.5}$ in the MME. The largest model-spread among the five main $PM_{2.5}$ species comes from $PM_{2.5}$DU (Fig. 16), indicating its largest contribution to the $PM_{2.5}$ uncertainty over Asia.

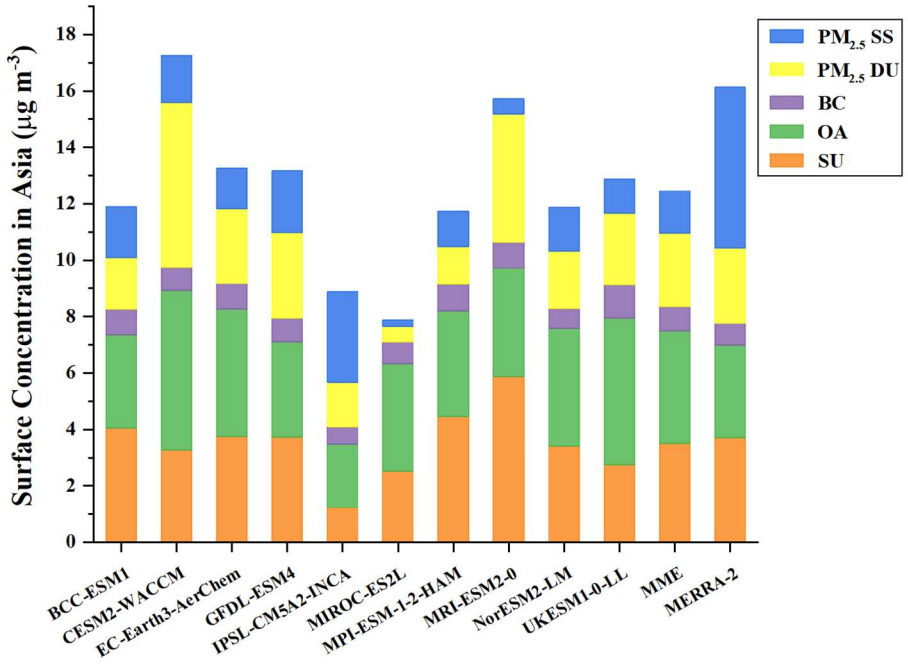

Fig. 15. Histograms of 2005–2020 averaged concentrations of $PM_{2.5}$ and their components (sulfate, organic aerosols, black carbon, $PM_{2.5}$DU, $PM_{2.5}$SS) from 10 ESMs, their MME, and MERRA-2 for Asia

(70–140° E, 5–55° N). Units: μg m^{-3}. The mean value in MME and model diversity for the five main $PM_{2.5}$ species are 3.5 ±1.23 μg m^{-3} for sulfate, 3.98 ±0.98 μg m^{-3} for OA, 0.86 ±0.15 μg m^{-3} for BC, 2.59 ±1.57 μg m^{-3} for $PM_{2.5}$DU and 1.5 ±0.83 μg m^{-3} for $PM_{2.5}$SS.

The proportion of each $PM_{2.5}$ component has large regional characteristics (Fig. 16). $PM_{2.5}$DU plays a dominant role over Central Asia, accounting for 70% of the $PM_{2.5}$ concentration. There are also considerable differences in $PM_{2.5}$DU model results over Central Asia and the uncertainty range is almost 25 μg m^{-3}. In East Asia, sulfate and OA are the main $PM_{2.5}$ species, and the uncertainty is mostly attributed to $PM_{2.5}$DU and sulfate. In South Asia, the uncertainty ranges are comparable for sulfate, OA and $PM_{2.5}$DU. In Southeast Asia, $PM_{2.5}$SS accounts for 35% of the $PM_{2.5}$ in the MME, and it has the largest contribution to the $PM_{2.5}$ uncertainties. Overall, it appears that the regions of large model diversity are consistent with high concentrations areas for the five components.

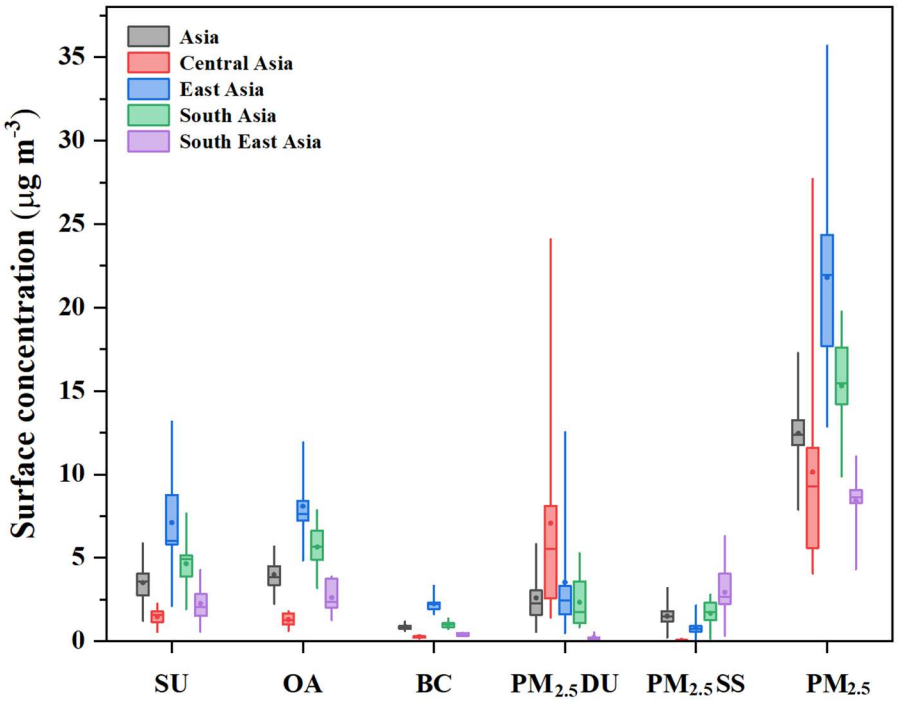

439 **Fig. 16.** The distribution of differences for $PM_{2.5}$ and their components (sulfate, OA, BC, $PM_{2.5}$DU,
440 $PM_{2.5}$SS) concentrations from 10 ESMs in Asia and four subregions during 2005-2020. The box plots
441 show the 25th and 75th percentiles as solid boxes, median values as solid lines, dots represent the
442 concentrations from MME, and whiskers extending to the minimum and maximum. Units: μg m^{-3}.

443

444 5. Uncertainties in evaluating $PM_{2.5}$ concentrations

445 The above analyses have shown that surface $PM_{2.5}$ concentrations from ESMs
446 simulations are lower than those from individual observations at CNEMC and EANET
447 sites. One possible reason is the spatial heterogeneity of ground-based observations and
448 the urban effect on $PM_{2.5}$ concentrations. It is noticed that all the CNEMC sites are
449 located in urban areas, whereas ESMs simulate average $PM_{2.5}$ concentrations across a
450 coarse model grid larger than 100 km and is hard to identify the differences between
451 urban and suburban area. Figure 17a shows time series of surface $PM_{2.5}$ concentrations
452 at one city and its neighboring suburban site in Thailand from APAD data (Cohen et
453 al., 2015). It is clear that the surface $PM_{2.5}$ concentrations at the urban location are
454 evidently higher than those at the neighboring suburban site. The urban site in Thailand
455 is in a residential-university-shopping district containing commercial buildings and
456 small industrial factories. The emissions mainly come from human activities (including
457 automobile exhausts, residential cooking and heating from buildings). By contrast, the
458 suburban site is surrounded by residential areas with brick-timbered houses, trees and
459 grass. Urban observatories are more polluted than suburban ones, even when they are
460 geographically close to each other. This is also evident in the two pairs of urban and
461 neighboring suburban sites in China (Fig. 17b and 17c). Differences between
462 downtown and suburban sites in the same city may be higher than 10 μg m^{-3}, and the
463 results in ESMs are closer to those at suburban sites.

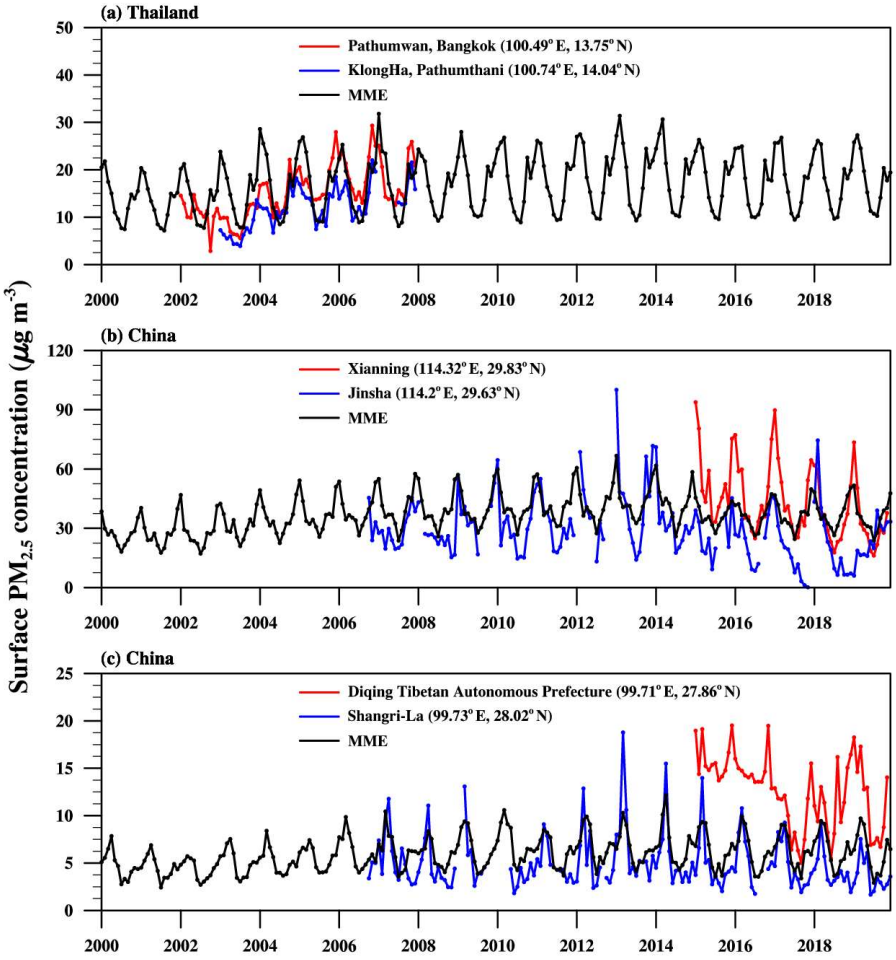

Fig. 17. Time series of surface $PM_{2.5}$ concentrations in neighboring city and suburb from APAD, CMA, CNEMC and MME. Red and blue lines represent observations at urban and suburban sites, respectively. Black lines represent the simulations from MME. Units: μg m^{-3}.

Another important reason for the uncertainty in evaluation is the method to calculate $PM_{2.5}$ concentrations. Firstly, Eq. (1) used in this study does not include all the aerosol components that constitute $PM_{2.5}$, such as ammonium and nitrate aerosols, which are generally included in observations but not model derived $PM_{2.5}$, especially important over eastern China where nitrate aerosols may be responsible for over 20% of $PM_{2.5}$ mass concentrations in winter (Liu et al., 2017). In addition, Eq. (1) assumes fixed percentages of the total mass of dust (10%) and sea salt (25%) aerosols present

476 within the fine size fraction (i.e., less than 2.5 microns in diameter), which are not
477 consistent among ESMs, and also is not suitable for the MERRA-2 data.
478

479 6. Summary

480 This study uses five main components of aerosols (i.e., sulfate, organic aerosol,
481 black carbon, dust and sea salt) that are simulated by ten CMIP6 ESMs to calculate
482 surface $PM_{2.5}$ concentrations over Asia. Ground-based observation networks as well as
483 the MERRA-2 reanalysis are used to evaluate the ability of current ESMs to simulate
484 $PM_{2.5}$ and its components. In Asia, $PM_{2.5}$ accounts for more than 30% of the total
485 aerosol (including all particle sizes), except for Central Asia. The spatial distribution of
486 $PM_{2.5}$ and its main components in the MME are in a good agreement with MERRA-2
487 and available ground-based observations. High $PM_{2.5}$ concentrations (> 40 μg m^{-3} in
488 MERRA-2) are simulated in three regions located in eastern China and in northern India
489 mainly consisting of anthropogenic aerosols, and in northwestern China due to high
490 concentrations of mineral dust. The contribution of each aerosol component to the
491 MME $PM_{2.5}$ across Asia are mainly from sulfate (28%), OA (32%), and $PM_{2.5}$DU
492 (21%). The proportions of components making up the MME $PM_{2.5}$ are also regionally
493 dependent. $PM_{2.5}$DU accounts for more than 70% of $PM_{2.5}$ in Central Asia and $PM_{2.5}$SS
494 for about 35% of $PM_{2.5}$ in Southeast Asia in the MME.

495 Our analysis shows that $PM_{2.5}$ from ESMs are biased low in the comparison
496 with ground-based observations. It may be partly due to the unevenly distributed
497 ground-based observations and the effect of urban areas, as well as the formula used to
498 derive the $PM_{2.5}$ concentrations in this work which does not consider the contributions
499 of nitrate and ammonium compounds. Compared to the MERRA-2 reanalysis data, the
500 MME underestimates $PM_{2.5}$ concentrations averaged across Asia by about 3.7 μg m^{-3},

501 which is possibly due to large $PM_{2.5}$SS overestimation in MERRA-2.

502 There are large uncertainties in simulations of $PM_{2.5}$ and its components among
503 the 10 ESMs. Inter-model differences in $PM_{2.5}$ are mainly attributed to sulfate and
504 $PM_{2.5}$DU over East Asia, and $PM_{2.5}$DU over Central Asia. For South Asia, the
505 uncertainty ranges are comparable for sulfate, OA and $PM_{2.5}$DU. $PM_{2.5}$SS has the
506 largest uncertainty range in Southeast Asia. The differences in the simulation of $PM_{2.5}$
507 and its components amongst the 10 ESMs to a large extent reflect the different
508 algorithms used to prognose aerosol variations in the individual ESMs including the
509 dynamic transport, dry deposition, gravitational settling, wet scavenging, chemical
510 processes, meteorological drivers, land surface conditions, and the representation of
511 aerosol size distributions.

512 **This work is the first to highlight ESM model biases in the simulation of**
513 **$PM_{2.5}$ concentrations across Asia using observations and a reanalysis dataset.**
514 **Analyzing the individual aerosol components highlights the potential**
515 **improvements to ESMs and the certain aspects of their individual aerosol schemes**
516 **to target.** It is noted that the ground-based observations used in this work are relatively
517 sparse. The regional feature for $PM_{2.5}$ and its components in ESMs still needs further
518 investigations using more data with high spatial and time resolutions that retrieved from
519 satellite observations (Wei et al., 2020; Yan et al., 2020, 2021) in the future.

520

521 ***Acknowledgments.*** We would like to thank Meteorological Observation Center, China
522 Meteorological Administration for providing surface $PM_{2.5}$ data at atmospheric
523 background stations.

524

525 # References

526 Apte, J. S., J. D. Marshall, A. J. Cohen, et al., 2015: Addressing Global Mortality from
527 Ambient PM2.5. *Environ. Sci. Technol.*, **49**, 8057–8066, doi:
528 10.1021/acs.est.5b01236.
529 Aryal, Y. N., and S. Evans, 2021: Global Dust Variability Explained by Drought
530 Sensitivity in CMIP6 Models. *J. Geophys. Res. Earth Surf.*, **126**, 1–20, doi:
531 10.1029/2021JF006073.
532 Bollasina, M. A., Y. Ming, and V. Ramaswamy, 2011: Anthropogenic aerosols and the
533 weakening of the south asian summer monsoon. *Science*, **334**, 502–505, doi:
534 10.1126/science.1204994.
535 Bond, T. C., S. J. Doherty, D. W. Fahey, et al., 2013: Bounding the role of black carbon
536 in the climate system: A scientific assessment. *J. Geophys. Res. Atmos.*, **118**,
537 5380–5552, doi: 10.1002/jgrd.50171.
538 Boucher, O., S. Denvil, G. Levavasseur, et al., 2020a: IPSL IPSL-CM5A2-INCA model
539 output prepared for CMIP6 CMIP historical. Earth System Grid Federation. doi:
540 10.22033/ESGF/CMIP6.13661.
541 Boucher, O., S. Denvil, G. Levavasseur, et al., 2020b: IPSL IPSL-CM5A2-INCA
542 model output prepared for CMIP6 ScenarioMIP ssp370. Earth System Grid
543 Federation. doi: 10.22033/ESGF/CMIP6.15714.
544 Buchard, V., A. M. da Silva, C. A. Randles, et al., 2016: Evaluation of the surface
545 PM2.5 in Version 1 of the NASA MERRA Aerosol Reanalysis over the United
546 States. *Atmos. Environ.*, **125**, 100–111, doi: 10.1016/j.atmosenv.2015.11.004.
547 Buchard, V., C. A. Randles, A. M. Da Silva, et al., 2017: The MERRA-2 aerosol
548 reanalysis, 1980 onward. Part II: Evaluation and case studies. *J. Climate*, **30**,
549 6851–6872, doi: 10.1175/JCLI-D-16-0613.1.
550 Charlson, R. J., S. E. Schwartz, J. M. Hales, et al., 1992: Climate forcing by

551 anthropogenic aerosols. *Science*, **255**, 423–430, doi:
552 10.1126/science.255.5043.423.
553 Coakley, J. A., R. D. Cess, and F. B. Yurevich, 1983: The Effect of Tropospheric
554 Aerosols on the Earth's Radiation Budget: A Parameterization for Climate Models.
555 *J. Atmos. Sci.*, **40**, 116–138, doi: 10.1175/1520-
556 0469(1983)040<0116:TEOTAO>2.0.CO;2.
557 Cohen, D. D., and A. J. Atanacio, 2015: The IAEA/RCA Fine and Coarse Particle
558 Ambient Air Database. ANSTO Report/E-784, Australia, Australian Nuclear
559 Science and Technology Organisation, 1-35. Collins, W. J., J. F. Lamarque, M.
560 Schulz, et al., 2017: AerChemMIP: Quantifying the effects of chemistry and
561 aerosols in CMIP6. *Geosci. Model Dev.*, **10**, 585–607, doi: 10.5194/gmd-10-585-
562 2017.
563 Danabasoglu, G., 2019a: NCAR CESM2-WACCM model output prepared for CMIP6
564 CMIP historical. Earth System Grid Federation. doi:
565 10.22033/ESGF/CMIP6.10071.
566 Danabasoglu, G., 2019b: NCAR CESM2-WACCM model output prepared for CMIP6
567 ScenarioMIP ssp370. Earth System Grid Federation. doi:
568 10.22033/ESGF/CMIP6.10102.
569 Danabasoglu, G., J. F. Lamarque, J. Bacmeister, et al., 2020: The Community Earth
570 System Model Version 2 (CESM2). *J. Adv. Model. Earth Syst.*, **12**,
571 e2019MS001916, doi: 10.1029/2019MS001916.
572 Dunne, J. P., L. W. Horowitz, A. J. Adcroft, et al., 2020: The GFDL Earth System
573 Model Version 4.1 (GFDL-ESM 4.1): Overall Coupled Model Description and
574 Simulation Characteristics. *J. Adv. Model. Earth Syst.*, **12**, e2019MS002015, doi:
575 10.1029/2019MS002015.

576 EC-Earth Consortium (EC-Earth), 2020a: EC-Earth-Consortium EC-Earth3-AerChem
577 model output prepared for CMIP6 CMIP historical. Earth System Grid Federation.
578 doi: 10.22033/ESGF/CMIP6.4701.
579 EC-Earth Consortium (EC-Earth), 2020b: EC-Earth-Consortium EC-Earth3-AerChem
580 model output prepared for CMIP6 ScenarioMIP ssp370. Earth System Grid
581 Federation. doi: 10.22033/ESGF/CMIP6.4885.
582 Eyring, V., S. Bony, G. A. Meehl, et al., 2016: Overview of the Coupled Model
583 Intercomparison Project Phase 6 (CMIP6) experimental design and organization.
584 *Geosci. Model Dev.*, **9**, 1937–1958, doi:10.5194/gmd-9-1937-2016.
585 Good, P., A. Sellar, Y. Tang, et al., 2019: MOHC UKESM1.0-LL model output
586 prepared for CMIP6 ScenarioMIP ssp370. Earth System Grid Federation. doi:
587 10.22033/ESGF/CMIP6.6347.
588 Guo, J. P., H. Liu, Z. Q. Li, et al., 2018: Aerosol-induced changes in the vertical
589 structure of precipitation: A perspective of TRMM precipitation radar. *Atmos.*
590 *Chem. Phys.*, **18**, 13329–13343, doi: 10.5194/acp-18-13329-2018.
591 Hajima, T., M. Abe, O. Arakawa, et al., 2019: MIROC MIROC- ES2L model output
592 prepared for CMIP6 historical. Earth System Grid Federation. doi:
593 10.22033/ESGF/CMIP6.5602.
594 Hajima, T., M. Watanabe, A. Yamamoto, et al., 2020: Development of the MIROC-
595 ES2L Earth system model and the evaluation of biogeochemical processes and
596 feedbacks. *Geosci. Model Dev.*, **13**, 2197–2244, doi: 10.5194/gmd-13-2197-2020.
597 Haywood, J. M., N. Bellouin, A. Jones, et al., 2011: The roles of aerosol, water vapor
598 and cloud in future global dimming/brightening. *J. Geophys. Res. Atmos.*, **116,**
599 D20203, doi: 10.1029/2011JD016000.
600 Hoesly, R. M., S. J. Smith, L. Feng, et al., 2018: Historical (1750-2014) anthropogenic

emissions of reactive gases and aerosols from the Community Emissions Data System (CEDS). *Geosci. Model Dev.*, **11**, 369–408, doi: 10.5194/gmd-11-369-2018.

Horowitz, L. W., V. Naik, F. Paulot, et al., 2020: The GFDL Global Atmospheric Chemistry-Climate Model AM4.1: Model Description and Simulation Characteristics. *J. Geophys. Res. Atmos.*, **12**, e2019MS002032, doi: 10.1029/2019MS002032.

Huijnen, V., J. Williams, M. Van Weele, et al., 2010: The global chemistry transport model TM5: Description and evaluation of the tropospheric chemistry version 3.0. *Geosci. Model Dev.*, **3**, 445–473, doi: 10.5194/gmd-3-445-2010.

Hwang, Y. T., D. M. W. Frierson, and S. M. Kang, 2013: Anthropogenic sulfate aerosol and the southward shift of tropical precipitation in the late 20th century. *Geophys. Res. Lett.*, **40**, 2845–2850, doi: 10.1002/grl.50502.

Jacobson, M. Z., 2001: Strong radiative heating due to the mixing state of black carbon in atmospheric aerosols. *Nature*, **409**, 695–697, doi: 10.1038/35055518.

John, J. G., C. Blanton, C. McHugh, et al., 2018: NOAA-GFDL GFDL-ESM4 model output prepared for CMIP6 ScenarioMIP ssp370. Earth System Grid Federation. doi: 10.22033/ESGF/CMIP6.8691.

Kirkeväg, A., A. Grini, D. Olivié, et al., 2018: A production-tagged aerosol module for earth system models, OsloAero5.3-extensions and updates for CAM5.3-Oslo. *Geosci. Model Dev.*, **11**, 3945–3982, doi: 10.5194/gmd-11-3945-2018.

Krasting, J. P., J. G. John, C. Blanton, et al., 2018: NOAA-GFDL GFDL-ESM4 model output prepared for CMIP6 CMIP historical. Earth System Grid Federation. doi: 10.22033/ESGF/CMIP6.8597.

Krol, M., S. Houweling, B. Bregman, et al., 2005: The two-way nested global

626 chemistry-transport zoom model TM5: Algorithm and applications. *Atmos. Chem.*
627 *Phys.*, **5**, 417–432, doi: 10.5194/acp-5-417-2005.
628 Lamarque, J. F., D. T. Shindell, B. Josse, et al., 2013: The atmospheric chemistry and
629 climate model intercomparison Project (ACCMIP): Overview and description of
630 models, simulations and climate diagnostics. *Geosci. Model Dev.*, **6**, 179–206, doi:
631 10.5194/gmd-6-179-2013.
632 Lau, K. M., M. K. Kim, and K. M. Kim, 2006: Asian summer monsoon anomalies
633 induced by aerosol direct forcing: The role of the Tibetan Plateau. *Climate Dyn.*,
634 **26**, 855–864, doi: 10.1007/s00382-006-0114-z.
635 Li, X., Y. W. Liu, M. H. Wang, et al., 2021: Assessment of the Coupled Model
636 Intercomparison Project phase 6 (CMIP6) Model performance in simulating the
637 spatial-temporal variation of aerosol optical depth over Eastern Central China.
638 *Atmos. Res.*, **261**, 105747, doi:10.1016/j.atmosres.2021.105747.
639 Li, Z. Q., F. Niu, J. W. Fan, et al., 2011: Long-term impacts of aerosols on the vertical
640 development of clouds and precipitation. *Nat. Geosci.*, **4**, 888–894, doi:
641 10.1038/ngeo1313.
642 Li, Z. Q., J. P. Guo, A. J. Ding, et al., 2017: Aerosol and boundary-layer interactions
643 and impact on air quality. *Natl. Sci. Rev.*, **4**, 810–833, doi: 10.1093/nsr/nwx117.
644 Lim, S. S., T. Vos, A. D. Flaxman, et al., 2012: A comparative risk assessment of
645 burden of disease and injury attributable to 67 risk factors and risk factor clusters
646 in 21 regions, 1990-2010: A systematic analysis for the Global Burden of Disease
647 Study 2010. *Lancet*, **380**, 2224–2260, doi: 10.1016/S0140-6736(12)61766-8.
648 Liu, H. B., R. J. Yan, and J. Yang, 2021: Credibility and statistical characteristics of
649 CAMSRA and MERRA-2 AOD reanalysis products over the Sichuan Basin during
650 2003–2018. *Atmos. Environ.*, **244,** 117980, doi: 10.1016/j.atmosenv.2020.117980.

651 Liu R. J., H. Liao, W. Y. Chang, et al., 2017: Impact of climate change on aerosol
652 concentrations in eastern China based on Atmospheric Chemistry and Climate
653 Model Intercomparison Project (ACCMIP) datasets. *Chinese J. Atmos. Sci.*, **41**,
654 739–751, doi:10.3878/j.issn.1006-9895.1612.16218. (in Chinese)
655 Liu, X., P. L. Ma, H. Wang, et al., 2016: Description and evaluation of a new four-
656 mode version of the Modal Aerosol Module (MAM4) within version 5.3 of the
657 Community Atmosphere Model. *Geosci. Model Dev.*, **9**, 505–522, doi:
658 10.5194/gmd-9-505-2016.
659 Menon, S., J. Hansen, L. Nazarenko et al., 2002: Climate effects of black carbon
660 aerosols in China and India. *Science*, **297**, 2250–2253, doi:
661 10.1126/science.1075159.
662 Mulcahy, J. P., C. Johnson, C. G. Jones, et al., 2020: Description and evaluation of
663 aerosol in UKESM1 and HadGEM3-GC3.1 CMIP6 historical simulations. *Geosci.*
664 *Model Dev.*, **13**, 6383-6423, doi: 10.5194/gmd-13-6383-2020.
665 Neubauer, D., S. Ferrachat, D. C. Siegenthaler-Le, et al., 2019a: HAMMOZ-
666 Consortium MPI-ESM1.2-HAM model output prepared for CMIP6 CMIP
667 historical. Earth System Grid Federation. doi: 10.22033/ESGF/CMIP6.5016.
668 Neubauer, D., S. Ferrachat, D. C. Siegenthaler-Le, et al., 2019b: HAMMOZ-
669 Consortium MPI-ESM1.2-HAM model output prepared for CMIP6
670 AerChemMIP. Earth System Grid Federation. doi: 10.22033/ESGF/CMIP6.1621.
671 Oshima, N., S. Yukimoto, M. Deushi, et al., 2020: Global and Arctic effective radiative
672 forcing of anthropogenic gases and aerosols in MRI-ESM2.0. *Prog. Earth Planet.*
673 *Sci.*, **7**, 1-21, doi: 10.1186/s40645-020-00348-w.
674 Ramanathan, V., P. J. Crutzen, J. T. Kiehl, et al., 2001: Aerosols, Climate, and the
675 Hydrological Cycle. *Science*, **294**, 2119–2124, doi: 10.1126/science.1064034.

676 Randles, C. A., A. M. Da Silva, V. Buchard, et al., 2017: The MERRA-2 aerosol
677 reanalysis, 1980 onward. Part I: System description and data assimilation
678 evaluation. *J. Clim.*, **30**, 6823–6850, doi: 10.1175/JCLI-D-16-0609.1.
679 Seland, Ø., M. Bentsen, D. Olivié, et al., 2019a: NCC NorESM2-LM model output
680 prepared for CMIP6 CMIP historical. Earth System Grid Federation. doi:
681 10.22033/ESGF/CMIP6.8036.
682 Seland, Ø., M. Bentsen, D. Olivié, et al., 2019b: NCC NorESM2-LM model output
683 prepared for CMIP6 ScenarioMIP ssp370. Earth System Grid Federation. doi:
684 10.22033/ESGF/CMIP6.8268.
685 Seland, Ø., M. Bentsen, D. Olivié, et al., 2020: Overview of the Norwegian Earth
686 System Model (NorESM2) and key climate response of CMIP6 DECK, historical,
687 and scenario simulations. *Geosci. Model Dev.,* **13**, 6165-6200, doi: 10.5194/gmd-
688 13-6165-2020.
689 Sellar, A. A., C. G. Jones, J. P. Mulcahy, et al., 2019: UKESM1: Description and
690 Evaluation of the U.K. Earth System Model. *J. Adv. Model. Earth Syst.*, **11**, 4513–
691 4558, doi: 10.1029/2019MS001739.
692 Sepulchre, P., A. Caubel, J. B. Ladant, et al., 2020: IPSL-CM5A2 - An Earth system
693 model designed for multi-millennial climate simulations. *Geosci. Model Dev.*, **13**,
694 3011–3053, doi: 10.5194/gmd-13-3011-2020.
695 Shi, Y., T. Matsunaga, Y. Yamaguchi, et al., 2018: Long-term trends and spatial
696 patterns of satellite-retrieved PM2.5 concentrations in South and Southeast Asia
697 from 1999 to 2014. *Sci. Total Environ.*, **615**, 177–186, doi:
698 10.1016/j.scitotenv.2017.09.241.
699 Silva, R. A., J. J. West, Y. Zhang, et al., 2013: Global premature mortality due to
700 anthropogenic outdoor air pollution and the contribution of past climate change.

Environ. Res. Lett., **8**, 034005, doi: 10.1088/1748-9326/8/3/034005.

Singh, N., V. Murari, M. Kumar, et al., 2017: Fine particulates over South Asia: Review and meta-analysis of PM2.5 source apportionment through receptor model. *Environ. Pollut.*, **223**, 121–136, doi: 10.1016/j.envpol.2016.12.071.

Sweerts, B., S. Pfenninger, S. Yang, et al., 2019: Estimation of losses in solar energy production from air pollution in China since 1960 using surface radiation data. *Nat. Energy.*, **4**, 657–663, doi: 10.1038/s41560-019-0412-4.

Szopa, S., Y. Balkanski, M. Schulz, et al., 2013: Aerosol and ozone changes as forcing for climate evolution between 1850 and 2100. *Clim. Dyn.*, **40**, 2223–2250, doi: 10.1007/s00382-012-1408-y.

Tachiiri, K., M. Abe, T. Hajima, et al., 2019: MIROC MIROC-ES2L model output prepared for CMIP6 ScenarioMIP ssp370. Earth System Grid Federation. doi: 10.22033/ESGF/CMIP6.5751.

Takemura, T., H. Okamoto, Y. Maruyama, et al., 2000: Global three-dimensional simulation of aerosol optical thickness distribution of various origins. *J. Geophys. Res. Atmos.*, **105**, 17853–17873, doi: 10.1029/2000JD900265.

Takemura, T., T. Nozawa, S. Emori, et al., 2005: Simulation of climate response to aerosol direct and indirect effects with aerosol transport-radiation model. *J. Geophys. Res.*, **110**, D02202, doi:10.1029/2004JD005029.

Takemura, T., M. Egashira, K. Matsuzawa, et al., 2009: A simulation of the global distribution and radiative forcing of soil dust aerosols at the Last Glacial Maximum. *Atmos. Chem. Phys.*, **9**, 3061–3073, doi: 10.5194/acp-9-3061-2009.

Tang, Y., S. Rumbold, R. Ellis, et al., 2019: MOHC UKESM1.0-LL model output prepared for CMIP6 CMIP historical. Earth System Grid Federation. doi: 10.22033/ESGF/CMIP6.6113.

726 Tegen, I., D. Neubauer, S. Ferrachat, et al., 2019: The global aerosol-climate model
727 echam6.3-ham2.3 -Part 1: Aerosol evaluation. *Geosci. Model Dev.*, **12**, 1643–
728 1677, doi: 10.5194/gmd-12-1643-2019.
729 Textor, C., M. Schulz, S. Guibert, et al., 2007: The effect of harmonized emissions on
730 aerosol properties in global models - An AeroCom experiment. *Atmos. Chem.*
731 *Phys.*, **7**, 4489–4501, doi:10.5194/acp-7-4489-2007.
732 Tosca, M. G., J. T. Randerson, C. S. Zender, et al., 2010: Do biomass burning aerosols
733 intensify drought in equatorial Asia during El Niño? *Atmos. Chem. Phys.*, **10**,
734 3515–3528, doi: 10.5194/acp-10-3515-2010.
735 Turnock, S. T., R. J. Allen, M. Andrews, et al., 2020: Historical and future changes in
736 air pollutants from CMIP6 models. *Atmos. Chem. Phys.*, **20**, 14547–14579, doi:
737 10.5194/acp-20-14547-2020.
738 Ukhov, A., S. Mostamandi, A. da Silva, et al., 2020: Assessment of natural and
739 anthropogenic aerosol air pollution in the Middle East using MERRA-2, CAMS
740 data assimilation products, and high-resolution WRF-Chem model simulations.
741 *Atmos. Chem. Phys.*, **20**, 9281–9310, doi:10.5194/acp-20-9281-2020.
742 Van Noije, T., T. Bergman, P. Le Sager, et al., 2021: EC-Earth3-AerChem: A global
743 climate model with interactive aerosols and atmospheric chemistry participating
744 in CMIP6. *Geosci. Model Dev.*, **14**, 5637–5668, doi: 10.5194/gmd-14-5637-2021.
745 Wang M. X., and R. J. Zhang, 2001: Frontier of Atmospheric Aerosols Researches.
746 Climatic Environ. Res., 6, 119-124, doi: 10.3969/j.issn.1006-9585.2001.01.014.
747 (in Chinese)
748 Wang, Y., Q. Wan, W. Meng, et al., 2011: Long-term impacts of aerosols on
749 precipitation and lightning over the Pearl River Delta megacity area in China.
750 *Atmos. Chem. Phys.*, **11**, 12421–12436, doi:10.5194/acp-11-12421-2011.

751 Wang, Y., A. Khalizov, M. Levy, et al., 2013: New Directions: Light absorbing aerosols
752 and their atmospheric impacts. *Atmos. Environ.*, **81**, 713–715, doi:
753 10.1016/j.atmosenv.2013.09.034.
754 Wei, J., Z. Q. Li, M. Cribb, et al., 2020: Improved 1km resolution PM2.5 estimates
755 across China using enhanced space-time extremely randomized trees. *Atmos.*
756 *Chem. Phys.*, **20**, 3273–3289, doi:10.5194/acp-20-3273-2020.
757 Wei, Y., X. S. Chen, H. S. Chen, et al., 2019: IAP-AACM v1. 0: a global to regional
758 evaluation of the atmospheric chemistry model in CAS-ESM, *Atmos. Chem. Phys.*,
759 **19**, 8269–8296, doi: 10.5194/acp-19-8269-2019.
760 Wilcox, L. J., Z. Liu, B. H. Samset, et al., 2020: Accelerated increases in global and
761 Asian summer monsoon precipitation from future aerosol reductions. *Atmos.*
762 *Chem. Phys.,* **20**, 11955–11977, doi: 10.5194/acp-20-11955-2020.
763 Witek, M. L., P. J. Flatau, P. K. Quinn, et al., 2007: Global sea-salt modeling: Results
764 and validation against multicampaign shipboard measurements. *J. Geophys. Res.*
765 *Atmos.*, **112**, D08215, doi: 10.1029/2006JD007779.
766 Wu, G. X., Z. Q. Li, C. B. Fu, et al., 2016a: Advances in studying interactions between
767 aerosols and monsoon in China. *Sci. China Earth Sci.*, **59,** 1–16, doi:
768 10.1007/s11430-015-5198-z.
769 Wu, J., Y. Xu, and B. T. Zhou, 2016b: The Evaluation of Surface PM2.5 Concentration
770 over China Based on ACCMIP Models. *Clim. Chang. Res.*, **12**, 268-275,
771 doi:10.12006/j.issn.1673-1719.2015.188. (in Chinese)
772 Wu, T. W., F. Zhang, J. Zhang, et al., 2020: Beijing Climate Center Earth System Model
773 version 1 (BCC-ESM1): Model description and evaluation of aerosol simulations.
774 *Geosci. Model Dev.*, **13**, 977–1005, doi:/10.5194/gmd-13-977-2020.
775 Yan, X., Z. Zang, N. N. Luo, et al., 2020: New interpretable deep learning model to

776 monitor real-time PM2.5 concentrations from satellite data. *Environ. Int.*, **144**,
777 106060, doi: 10.1016/j.envint.2020.106060.
778 Yan, X., Z. Zang, C. Liang, et al., 2021: New global aerosol fine-mode fraction data
779 over land derived from MODIS satellite retrievals. *Environ. Pollut.*, **276**, 116707,
780 doi: 10.1016/j.envpol.2021.116707.
781 Yukimoto, S., H. Kawai, T. Koshiro, et al., 2019a: The meteorological research institute
782 Earth system model version 2.0, MRI-ESM2.0: Description and basic evaluation
783 of the physical component. *J. Meteor. Soc. Japan*, **97**, 931–965, doi:
784 10.2151/jmsj.2019-051.
785 Yukimoto, S., T. Koshiro, H. Kawai, et al., 2019b: MRI MRI-ESM2.0 model output
786 prepared for CMIP6 CMIP historical. Earth System Grid Federation. doi:
787 10.22033/ESGF/CMIP6.6842.
788 Yukimoto, S., T. Koshiro, H. Kawai, et al., 2019c: MRI MRI-ESM2.0 model output
789 prepared for CMIP6 ScenarioMIP ssp370. Earth System Grid Federation. doi:
790 10.22033/ESGF/CMIP6.6915.
791 Zhang, H., X. Y. Ma, S. Y. Zhao, et al., 2021: Advances in research on the ITCZ: Mean
792 position, model bias, and anthropogenic aerosol influences. *J. Meteor. Res.*, **35**,
793 729–742, doi: 10.1007/s13351-021- 0203-2.
794 Zhang, J., T. W. Wu, X. L. Shi, et al., 2018: BCC BCC-ESM1 model output prepared
795 for CMIP6 CMIP historical. Earth System Grid Federation. doi:
796 10.22033/ESGF/CMIP6.2949.
797 Zhang, J., T. W. Wu, X. L. Shi, et al., 2019a: BCC BCC-ESM1 model output prepared
798 for CMIP6 AerChemMIP ssp370. Earth System Grid Federation. doi:
799 10.22033/ESGF/CMIP6.3036.
800 Zhang, R., G. Li, J. Fan, et al., 2007: Intensification of Pacific storm track linked to

801 Asian pollution. *Proc. Natl. Acad. Sci. U. S. A.*, **104**, 5295–5299, doi:
802 10.1073/pnas.0700618104.
803 Zhang, Y., Y. N. Li, J. P. Guo, et al., 2019b: The climatology and trend of black carbon
804 in China from 12-year ground observations. *Climate Dyn.*, **53**, 5881–5892, doi:
805 10.1007/s00382-019-04903-0.
806 Zhang, Y., J. L. Jin, P. Yan, et al., 2020: Long-term variations of major atmospheric
807 compositions observed at the background stations in three key areas of China. *Adv.*
808 *Clim. Chang. Res.*, **11**, 370–380, doi: 10.1016/j.accre.2020.11.005.
809 Zhao, A., C. L. Ryder, and L. J. Wilcox, 2022: How well do the CMIP6 models simulate
810 dust aerosols? *Atmos. Chem. Phys.*, **22**, 2095–2119, doi: 10.5194/acp-22-2095-
811 2022.
812 Zhao, X., R. J. Allen, and E. S. Thomson, 2021: An Implicit Air Quality Bias Due to
813 the State of Pristine Aerosol. *Earth's Futur.*, **9**, e2021EF001979,
814 doi:10.1029/2021EF001979.